Isabella Radl

Sensitivity of structural connectivity in patients with ALS

Master Thesis

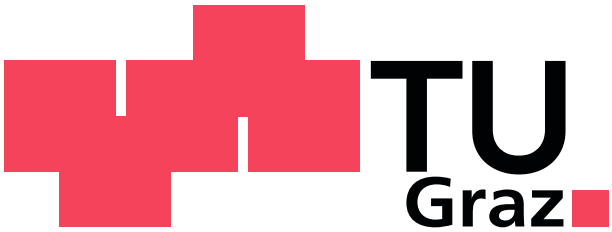

Institute for Medical Engineering
Technical University of Graz
Kronesgasse 5/II
A-8010 Graz
Head of the Institute: Univ.-Prof. Dr.techn. Dipl.-Ing. Rudolf Stollberger

Advisor: Dipl.-Ing. Dr.techn. Christian Langkammer
Reviewer: Univ.-Prof. Dipl.-Ing. Dr.techn. Rudolf Stollberger

Graz, (April 22, 2015)

Danke, Mama und Papa

Danke, Carina

Danke, Christian

Danke, Florian, Lukas, Johannes, Christoph, Prof. Ropele und Prof. Stollberger

Danke, Spane und Martin

Abstract

Although the brain is one of the most complex and investigated systems, its underlying structural relations and related functions are still not fully resolved. Structural connectivity is a novel field of research which models the complexity and interaction of distinct regions of the brain mathematically - as a network.
The aim of this thesis was to investigate structural connectivity in amyotrophic lateral sclerosis (ALS), its relation to normal brain, and whether it bears the potential as an additional marker for diagnosis and disease progression. Therefore structural connectivity was investigated with methods of diffusion magnetic resonance imaging at 3T and the structural networks were further analyzed with methods of graph theory to assess differences between 31 patients with ALS and 34 controls.
Group analysis found a region of different connectivity between ALS and controls, which spatially overlapped with the right corticospinal-tract. Additionally the strength of structural connectivity correlated with ALS disease progression ($r = 0.4$).
In conclusion, the analysis of structural connectivity identified disease related changes in a subnetwork of the brain and revealed a novel marker for disease progression. The location of this subnetwork extends well-known findings in the mesencephalic corticospinal-tract by an additional involvement of cortical regions.

Kurzfassung

Obwohl das Gehirn eines der komplexesten und zugleich am meisten erforschten Systeme ist, sind die strukturelle Konnektivität und das Zusammenspiel der einzelnen Bausteine noch nicht endgültig geklärt. Strukturelle Konnektivität ist ein neues Forschungsfeld, welches die Komplexität und Interaktion der verschiedenen Gehirnregionen mathematisch modelliert – als Netzwerk.
Das Ziel dieser Arbeit war es, strukturelle Konnektivität bei Amyotropher Lateralsklerose (ALS) zu untersuchen, diese in Verbindung mit gesunden Gehirnen zu bringen, und zu untersuchen, ob diese als zusätzlicher Marker in Diagnose und Fortschreiten der Krankheit verwendet werden kann. Strukturelle Konnektivität wurde mit Methoden der Diffusions Magnetresonanzbildgebung bei 3T untersucht. Um Unterschiede zwischen 31 ALS Patienten und 34 Kontrollen zu finden, wurden die strukturellen Netzwerke mit Methoden der Graphentheorie untersucht.
Mittels Gruppenanalyse wurde ein betroffenes Areal mit veränderter Konnektivität zwischen ALS Patienten und Kontrollen gefunden, welches örtlich mit den Regionen des rechten Kortikospinaltraktes übereinstimmt. Des Weiteren korrelierte die Stärke der strukturellen Konnektivität signifikant mit dem Krankheitsverlauf ($r = 0.4$).
Zusammenfassend zeigte die Analyse der strukturellen Konnektivität krankheitsbezogene Veränderungen in einem Subnetzwerk des Gehirns und fand einen neuen Marker für das Fortschreiten der Krankheit. Der Ort des Subnetzwerks erweitert bereits bekannte Befunde des mesencephalen Kortikospinaltrakts mit einer zusätzlichen Beteiligung der kortikalen Regionen.

Contents

Statutory Declaration

I declare that I have authored this thesis independently, that I have not used other than the declared sources / resources, and that I have explicitly marked all material which has been quoted either literally or by content from the used sources.

Eidesstattliche Erklärung

Ich erkläre an Eides statt, dass ich die vorliegende Arbeit selbstständig verfasst, andere als die angegebenen Quellen/Hilfsmittel nicht benutzt und die den benutzten Quellen wörtlich und inhaltlich entnommene Stellen als solche kenntlich gemacht habe.

Ort	Datum	Unterschrift

1 Introduction

It is the age of networks. Social networks are part of our daily live, *networking* nowadays is an important skill in professional life and one of the biggest networks, the *world wide web* expands immensly every day. But what if *we* can be described by a network? What if we are nothing more than our brains connections? „I am my connectome“ is the famous teaser Sebastian Seung used in his book; stating that the neurons and connecting axons of our brain make us *who we are*.

To understand the most complex object in the known universe [66] a lot of research was done in the last decades. A huge project of the Washington University, University of Minnesota and Oxford University (the WU-Minn HCP consortium) - the *Human Connectome Project* - aims to map the connectomes (= brain-networks) of an immense number of humans to get an inside look into brains wiring. [70]

The field of *Connectomics* thus aims to generate networks describing our human brain. The intention behind it is, that we are able to identify and understand numerous diseases - of course with the previous knowledge of many healthy brain-networks. In short, it will „transform our understanding of the human brain in health and disease“. [70]

One of the most promising attempts to map the brain's connections is *Magnetic Resonance Imaging* - it is non-invasive, relatively fast and it resolves the brain's wiring.

The aim of this thesis is to generate such brain-networks with *MRI* and to analyse the obtained networks with methods of graph theory [59] and Network-based statistics [78]. The networks of healthy controls are compared with those of patients with ALS. To show if structural connectivity might be a better marker in disease diagnosis or progression, the

results are compared to the findings of other studies in the following sections.

2 Background

2.1 Diffusion MRI

The principle of Diffusion MRI is that diffusion of water *in white matter* is hindered and follows primarly along the path of axons. The result of dMRI is either a orientation distribution function (DSI,HARDI) or a main diffusion orientation vector (DTI) for each voxel. By following these vectors or probabilities of orientation one can get an idea of the main fiber tracts in the human brain.

2.1.1 Diffusion Tensor Imaging

The first and simpliest model was proposed 20 years ago of Peter Basser [6] and is called *Diffusion Tensor Imaging* (DTI).
It measures the signal attenuation due to strong gradients in different directions. If the measured voxel is part of a main fiber tract, water diffusion mainly follows along the path of axons and a strong signal attenuation is measured. Water molecules are restricted perpendicular to the fibre tract and less signal attenuation is measured. This signal attenuation S is modelled with the following equation.

$$S = S_0 \exp\left(-b\mathbf{D}\right) \tag{2.1}$$

where S_0 is the signal without diffusion gradients, b a measure of gradients strength and **D** is the *Diffusion Tensor* (shown in figure 2.1).

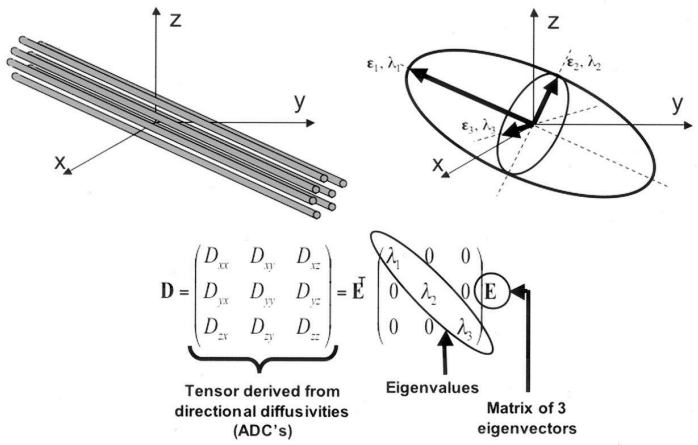

Figure 2.1: Diffusion Tensor, image taken from [45]

The diffusion tensor is symmetric and can be described with six independent parameters, therefore a minimum of six independent measurements are needed. By determing the eigenvalues and eigenvectors of this tensor, the main direction of water diffusion can be determined.

The eigenvalues and eigenvectors are used to calculate important measures in dMRI. These include *Fractional Anisotropy* (FA) and different diffusivities (mean diffusivity MD, axial and radial diffusivity AD, RD) The mean diffusivity is calculated as a third of the trace of the diffusion tensor (the „average trace“). The axial diffusion is described by the major eigenvalue and the radial diffusion contrary by the average of the two smaller eigenvalues. The fractional anisotropy measures the anisotropic fraction of the diffusion tensor, whereas a low fractional anisotropy indicates *isotropic tissue* and a high FA *anisotropic tissue*:

$$\mathrm{FA} = \sqrt{\frac{(\lambda_1 - \mathrm{MD})^2 + (\lambda_2 - \mathrm{MD})^2 + (\lambda_3)^2}{2(\lambda_1^2 + \lambda_2^2 + \lambda_3^2)}} \tag{2.2}$$

The fractional anisotropy is one of the most commonly used measures in DTI as it may reflect changes in myelination and organization of fibers. [1]

Nevertheless, DTI is not the gold standard of diffusion weighted image processing. Several assumptions, such as the fibre number per voxel, the gaussianity of the diffusion pattern and the fact that the most probable direction is taken as the main direction of diffusion (i.e. Maximum Likelihood assumption) make this method less applicable as newer methods have been developed.

2.1.2 Advanced Models Beyond DTI

To overcome the limitations of DTI several new methods were proposed. One can distinguish between model-based and model-free methods.

Model-based methods As the name suggests, model-based methods use a model to describe the diffusion pattern. The most popular method beyond DTI is the ball-and-stick model [11], which is described in detail in chapter 3.2.1.2. Free (isotropic) diffusion is modeled with a ball and the directed (anisotropic) diffusion in the axons with a stick.
Another method is called *Diffusion kurtosis imaging* which models the non-Gaussian characteristics of Diffusion with an additional parameter in equation 2.1.
Constrained spherical deconvolution (CSD) is a method which models the diffusion within a voxel by deconvoluting the MR signal and obtaining fiber orientation distribution functions as a superposition of spherical harmonics in every voxel. [48]
The main advantage of these methods is the relatively low requirement of diffusion sampling directions and thereby a reduced scanning time allowing clinical usage. The major drawback is certainly the assumptions of the diffusion models which might be violated in reality. [1]

Model-free methods *Model-free methods* obtain the empirical distribution of diffusion by exhaustive sampling. A distribution function is used to estimate the diffusion distribution in every voxel. Common model-free methods include q-space imaging or diffusion

spectrum imaging. [74] The major drawback of these methods is the need of a high number of diffusion gradient directions and multiple b-values. [1]

2.1.3 Fibertracking

Fibertracking describes a method for finding the trajectories of fiber bundles through white matter. It is done by determining the preferred direction of water diffusion and map it as a curve in three-dimensional space. The most simple and common approach is known as streamline tractography.

Deterministic Tracking Streamline algorithms start at one point - called the *seeding point* - and follow the main direction of diffusion in every voxel until a stopping criteria is met. The trajectory is therefore always tangent to the local main diffusion vector (major eigenvector of the diffusion tensor). This type of algorithm is called *deterministic* because it assumes a *single orientation* at each voxel. The uncertainty of the estimate is not regarded. Moreover, the simple method of creating a *streamline* is clearly a source of very obvious artifacts and additionally crossing fibers cannot be modelled with this simple approach. In DTI and streamline tractography only one fibre per voxel is assumed, therefore crossing or kissing fibers cannot be dissolved probably. An additional drawback is that crossing fibers can lead to reduced fractional anisotropy which often is a stopping criteria for streamline algorithms. Other methods based on a probabilistic approach were proposed in recent years to overcome these restrictions. [39]

Probabilistic Tracking Contrary to deterministic methods, *probabilistic* methods of fiber tracking regard the uncertainty of diffusion direction. Every voxel can have multiple diffusion directions, each with a different probability. The method of probabilistic fibre tracking is described in detail in section 3.2.1.2. [39]

2.2 The connectome

The term „Connectome“ was first stated by Olaf Sporns in 2005 [67] and simultaneously by Peter Hagmann [37]. Sporns defined the connectome as „structural description of the network of elements and connections forming the human brain“. [67] The idea behind is to get a look inside brains function by regarding its structural and functional connections.

Comparision to genomics *Connectome* is an artificial word, derived from the term *genome*, which is a complete listing of all nucleotide sequences, in the same way the *connectome* implies the *completeness* of all neural connections. The analysis of the structure and function of the connectome is (in the same way as it is with genomics) called *connectomics*. [55]
It is a relatively young field of science, genomics in contrast has a much longer tradition (starting in the late 70s), nevertheless the decryption of the whole human genome was possible in the first place only a few years ago. The human genome consists of 20000-30000 genes made from circa $3 \cdot 10^9$ base pairs, [67] in contrast the human brain consists of approximately 10^{11} neurons and 10^{16} connections, making the decryption a lot more challenging to realise. [38]

The three aspects in connectomics To really understand the term connectome it is a good idea to look at the formally given definition: There are three main aspects which define the connectome:
The *structural...* What is meant by structure? By definition structure is „the arrangement of and relations between the parts or elements of something complex“ [1]. In neuroscience, structure is related to the physical links between neural elements.
...description... is a compression of raw data to extract the maximal amount of infomation. An analogy would be the architectural description of a house: One would begin

[1] http://www.oxforddictionaries.com/definition/english/structure

by describing the main features not the exact building blocks or walls inside. The same is done in connectomics. A description provides an overview of the main features not the exact copy of all neurons and synapses.

...of the *network* of elements and connections forming the human brain. A network is a mathematical object consisting of elements and their connections. It is well known and studied by graph theory and therefore offers a large theoretical framework. [65]

Different scales A network is defined by its elements and connections: The smallest possible neural element would be a neuron, the connection a single synapse. As it was said previously the human brain consits of 10^{11} neurons. A network of this size (10^{11}x 10^{11} giving every possible connection) would not only be extremly hard to compute but also hard to analyze and interprete. If connectomes are resolved in this scale it is called „Microscale“.

In contrast, the „Macroscale“ defines elements of different *brain areas* and connections are described by *fibre tracts*. In contrast to neurons, which are easy to delineate, this is not given for a specific brain area or fiber tract. Furthermore, the number of distinct anatomical brain regions is still unknown. [78],[23],[67] The problem of dividing humans brain into distinct functional or structural areas is called *parcellation* and is further discussed in section 3.2.1.1.

Steps in Connectome Processing MRI is currently the best option to map connectomes in macroscale. It offers a non-invasive method which is able to capture the structural *and* functional connections of the human brain. [39] Structural connectomes can be generated with diffusion MRI (dMRI) by following the main diffusion direction in white matter, functional connectomes by acquiring a functional resting state MRI (fMRI/rsMRI). Resting state functional MRI measures spontaneous fluctuations in the so called BOLD (=*Blood-oxigenation-level-dependent*) signal in grey matter regions and computes cross-correlations between these BOLD time series.

In Sporns' first draft of the connectome [67] he proposed to generate a connectome of both the fMRI and dMRI data. Nevertheless, this thesis focusses structural connectivity as many studies have shown its validity before (e.g. [54], [71],[38]). [21],[65]

Intervariability The structural connectome is in general an invariant characteristic of our species but same as the genome it can show a high individual variation due to genetic differences, development and experiental history, gender differences or diseases. Another reason is the individual variability in size and location of different brain areas which makes a „standard connectome" hard to define. Besides the anatomical and functional differences in brains, methods of acquisition and processing might further impact the variability.

Outlook/Impact The connectome as a network should give a look inside the brains wiring, organization and maybe can be used as indicator for different diseases. Recent studies have shown the influence of diseases in the human connectome. [34],[8] Especially those which show myelin alteration or axonal degeneration and destruction (as for example *Amyotrophic Lateral Sclerosis ALS*, [71]) could have an influence on the human connectome.

2.3 ALS

Amyotrophic Lateral Sclerosis (ALS) - also known as Lou Gehring's disease - was first described by Charcot nearly 150 years ago in 1874. [58]
It is part of the whole group of motor neuron diseases which are characterised by progressive degeneration of motor neurones such as the *classical (Charcot's) ALS*, *progressive bulbar palsy* or *primary lateral sclerosis*. [75],[58]

2.3.1 Description of the disease

ALS is a neurodegenerative disease showing involvement of both upper and lower motor neurons. Upper motor neuron signs indicate that the affected region is above the anterior horn cells : i.e. motor cortex, brain stem and spinal cord; whereas lower motor neuron signs indicate that the disturbance is *in* or *distal* to the anterior horn cells. These cells can be found in the ventral part of the spinal cord and affect the axial muscles (figure 2.2). The symptoms of damage in the upper motor neuron cells, the *upper motor neuron signs*, are characterised by spasticities, weaknesses or increased reflexes. *Lower motor signs* appear with decreased muscle tone, arreflexia, weakness and a wasting in the muscle which is supplied by the diseased motor nerve. [69]

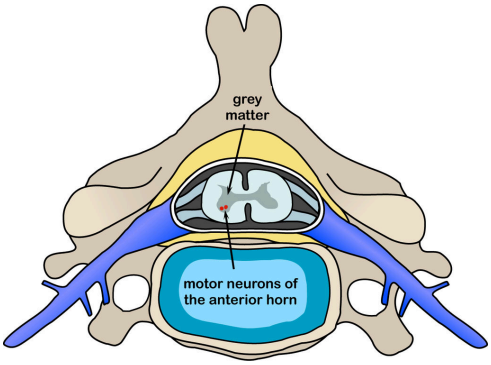

Figure 2.2: cross section of spinal cord showing anterior horn cells (marked as red points), image taken from [76].

The disease can thus be described as a *neurodegenerative disorder* which is „characterised by progressive muscular paralysis reflecting degeneration of motor neurons in the primary motor cortex, brainstem and spinal cord.“[75]
The term *Amyotrophy* refers to the atrophy of muscle fibres which are denervated because of the degeneration of anterior horn cells (lower motor neuron signs). *Lateral Sclerosis* describes the hardening of the anterior and lateral corticospinal tract. The hardening is caused by a proliferation of glial cells induced by degenerated motor neurons in this area.

Corticospinaltract

The corticospinal tract is the most important output pathway from the motor cortex. It originates about 30 per cent from the primary motor cortex, 30 per cent from the premotor and supplementary motor areas and 40 per cent from the somatosensory areas posterior to the central sulcus. (see figure 2.3) This major tract then passes through the posterior limb of the internal capsule (which is located between the caudate nucleus and the putamen of the basal ganglia) and descends through the brainstem where it forms the *pyramids in the medulla*. The pyramidal fibers pass through to the intermediate regions of the cord gray matter and build the ventral and lateral corticospinaltract. [35]

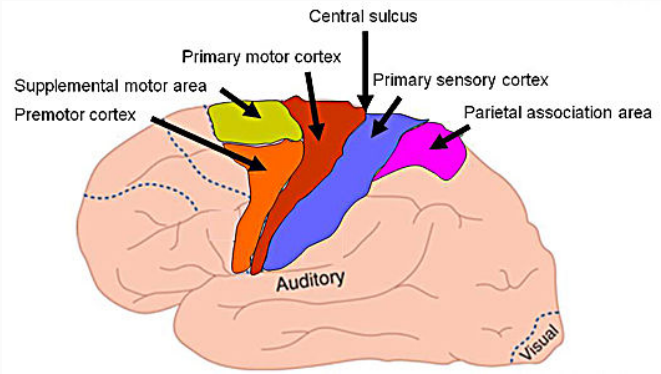

Figure 2.3: areas of corticospinal tract fibres, image adapted from [5]

The incidence of ALS has been reported in the 1990s between 1.5 and 2.7 per 100000 people/year in Europe and North America with an average age of onset between 55-65 years. It is a progressive disease with a mean survival time ranging from three to five years.

Patients often suffer from cramps, spasticity, excessive watery salvia, persistent salvia and bronchial secretions, excessive or violent yawning, laryngospasm, pain, emotional lability, communication difficulties, constipation, depression, insomnia, anxiety or fatigue. All of these symptomes can be treated to a certain extent but there is still no chance of healing. [75] Patients often die from respiratory failure three to five years after onset.

Although some genetic risk factors have been identified, the cause of ALS is still unknown.

Furthermore, *excitoxicity* which describes a neuronal injury induced by excessive glutamat induced stimulation, *oxidative stress* and *mitochondrial dysfunction* were found in patients with ALS. Moreover there may be impaired axonal transport, neurofilament and protein aggregation as part of the defence mechanism to reduce the intracellular concentration of toxic proteins, inflammatory dysfunction as well as dysfunction of signalling pathways. [58],[75]

With modern neuroimaging modalities it may be possible to better understand the pathophysiology of the disease in vivo and to identify potential biomarkers of disease progression to facilitate an earlier diagnosis. Thus, diffusion MRI can give a look inside into tissue's white matter microstructure and so may help to understand the pathological process of the disease. Several studies have been made in this area - a summary is presented in the following section.

2.3.2 Related Studies

Impaired Structural Motor Connectome in Amyotrophic Lateral Sclerosis - Verstraete et. al - 2011 [71]

The group of Verstraete studied the influence of ALS on FA (Fractional Anisotropy) - weighted connectivity maps. The entries of the connectome represent the mean *Fractional Anisotropy* (FA) along the found fibre tracts.

The participants involved 35 patients with ALS and 19 age-matched controls. They used diffusion tensor imaging (DTI) in connection with deterministic tracking (*FACT-Algorithm*: criteria: $FA > 0.1$,$\alpha < 45°$, $l > 30$mm). T_1 images where parcellated into 82 brain regions using *Freesurfer*. As next step all connections between region i and j were counted to fill the connectivity matrix. To control for false positives only connections (matrix entries) which were present in two thirds of *both* patients and controls where taken into account for further analysis. In contrast to the method used in this thesis, the entries of the connectivity matrix were filled with the average FA along the tracts, because they could reflect the microstructural organization of the tract.

For each FA-weighted-connectivity map several network measures including the *network strength S, the (normalized) average shortest path length L*, the *(normalized) average clustering coefficient C* and the *mean connectivity distribution* (i.e. a histogram of the connectome entries) were computed. Differences in these metrics were examined using permutation testing.

Additionally they examined *Network based statistics* [78] by using t-tests and 5000 permutations to create the null-distribution of the *maximal connected-component size*. The affected network was further investigated by computing the same network measures as before for the whole brain network and additionally some local network measures like *local efficiency Effi* and *node-specific connectivity strength* S_i. Possible associations between network measures of the impaired network and clinical scores (ALSFRS-R, and disease-progression) were examined using linear regression

They found no difference between ALS patients and controls in the overall graph metrics by studying the full connectome. An impaired network showing lower FA-connectivity values was found using *NBS* ($p = 0.01$). The affected regions of this network are listed in table 2.1. These regions strongly overlap with the known motor areas in the brain.

By examining the topology of the impaired network a significantly reduced level of network efficiency E and clustering was found in patients with ALS. However, the reduction in strength S was not statistically significant. Local measures showed significantly lower local efficiency in the left precentral, left caudal middlefrontal gyrus, the right paracentral, right precuneus and posterior cingulate gyrus.

The main finding of this study is therefore a reduced efficiency of a network strongly overlapping with bilateral motor regions such as precentral gyrus and paracentral lobule (BA 6) and supplementary motor regions (BA 4). Based on these findings they conclude that the center of the degenerative process of ALS may start in the primary motor regions but also effects suplementary regions as secondary motor connections. The focal damage in primary motor regions in ALS may ultimately manifest elsewhere in the brain.

Reduced Structural Connectivity Within a Prefrontal-Motor-Subcortical Network in Amyotrophic Lateral Sclerosis - Buchanan et al. - 2014 [15]

Buchanan et al. also studied FA-weighted connectomes of 30 ALS patients and 30 age-matched controls with NBS. They combined the findings of the study with TBSS. (Tract Based Spatial Statistics [63])

All dwMR images used in this study were acquired in 64 non-collinear directions ($b = 1000$ s /mm^2) along with 7 B_0 Images. The T_1 images were parcellated using *Freesurfer* and the *Desikan-Killiany* altlas [24] resulting in 34 cortical structures per hemisphere - plus brain-stem and eight other subcortical structures this resulted in 85 regions of interest. The diffusion weighted images were used to calculate the fractional anisotropy in each voxel for whole brain probabilistic tractography using FSLs BedpostX and ProbTrackX algorithm ([11], criteria: $\alpha < 70°, FA > 0.1, l > 200mm$). To reduce spurious connections a two step threshold was applied on the networks by first discarding the weakest 25% of weights for every connectivity matrix and after that retaining only connections which were present in at least 50% of all subjects. After this thresholding step different network measures of the FA-weighted networks like *network strength, clustering coefficient and efficiency* were computed.

Buchanan et al. used NBS to identify an impaired structural network and analysed the network found with this method further by relating it to the results found with TBSS - a skeletton-based analysis which is used to find differences in diffusion MR images (FA). Therefore they calculated the proportion of streamlines between nodes i and j which pass through any significant voxel identified by TBSS.

The impaired network consisted of 10 nodes and 12 connections (see table 2.1 for a listing of involved regions, $p = 0.020$) where all 12 connections are directly linked to nodes of the primary motor cortex. Three of these connections significantly correlated with disease progression rate.

TBSS analysis found significant reductions in FA within the corticospinal tract and part of the corpus callosum in patients. These regions strongly overlapped in 11 of the 12 connections. The global network measures showed no significant differences.

The main result is that connectivity in terms of tract-averaged FA is reduced in patients with ALS in primary motor, prefrontal and subcortical regions and that there is no brain-wide impairments in connectivity due to ALS.

Multimodal tract-based analysis in ALS patients at 7T: A specific white matter profile - Verstraete - 2014 [72]

The objective of this study was the exploration of the value of additional MR contrasts for studying ALS. For this reason eleven patients and nine controls were scanned at 3T and 7T to compare the results of diffusion weighted (3T), quantitative T_1 (qT_1), magnetization transfer ratio (MTR) and amide proton transfer weighted (APTw) imaging: Quantitative T_1 mapping can be used to asses the degree of myelination, as well as MTR which estimates the exchange of water bound to macromolecules and the unbound water fraction. The APTw imaging is done with the method of *chemical exchange saturation transfer* (CEST) which measures the exchange of protons between specific solutes and free water - if the protons are *amide* protons (chemical derivates of ammonia) the result is *amide proton transfer weighted imaging*. APTw is therefore expected to reflect physiological changes in this proton pool in case of ALS and has also shown to be sensitive for myelination. Beside these imaging techniques diffusion weighted images were acquired. Longitudinal and transversal diffusivity (D_{long}, D_{trans}) were calculated from DT data. The fiber tracking of the corticospinal tract (CST) was done by placing seed-regions in the left and right motor tract at the level of the pons with the following settings: $FA > 0.2$ $\alpha < 20°$, stepsize = 1 mm, $l_{min}/l_{max} = 40/500$ mm. Verstraete et al. performed a quantitative comparision of qT_1, MTR and APTw by registring each volume to the subject's FA map and doing a tract-based analysis by projecting the tracts of the CST to one single vertical curve and assigning the contrast of interest to the nearest voxels. The group average is calculated similarly by averaging the curves of all subjects.

No differences on the mean histograms of patients and controls for any of the different MR contrasts were found. The analysis of several MR measures along the CST revealed sig-

nificantly reduced FA, significantly higher transversal diffusivity D_{trans} and a significant increase of MTR in patients in the right CST. Changes in the left CST were not significant (see figure 2.4). No significant correlation was found between any MR parameters and clinical markers such as ALSFRS-R, progression or disease duration.
The reduction of FA is already known and was investigated earlier. [3] This finding is also consistent with the increase in transversal diffusivity. The decrease of the fractional anisotropy is known to indicate demyelination as it with the MTR. However this study demonstrates an *increase* in MTR. Buchanan et al. tried to explain this phenomenon with an accumulation of pathologic protein and an increased tissue liquid fraction. They claimed that the main reason for reduced FA is more likely the increase in the liquid fraction such as proliferation of glial cells and extracellular matrix expansion rather than demyelination.

Probabilistic diffusion tractography: A potential tool to assess the rate of disease progression in amyotrophic lateral sclerosis - Ciccarelli - 2006 [17]

This study based on a group of thirteen patients and nineteen controls, investigated the impact of ALS and disease duration and progression on voxel-based connectivity measures along the CST. They also investigated whether fractional anisotropy is reduced in patients and how it relates to disease progression rate.
Imaging for this study was performed on a 1.5T MRI System from GE. Diffusion weighted images were acquired with an DW-EPI sequence in 54 directions wtih an resolution of 1.7x1.7x2.3 mm^3 and a b-value of 1150 s/mm^2. Additionally, six B_0 and six images with a low weighting of $b = 300$ $mm/2^2$ were acquired to reconstruct the diffusion tensor from the combination of volumes with b_{min} and b_{max}. T_1 images were made with a resolution of 1.2x1.2x1.2 mm^3 using a 3D inversion-recovery prepared spoiled gradient recalled sequence.
The probabilstic tractography algorithm proposed of Behrens [11] was used to compute a voxel based connectivity index. Therefore the CST was delineated in each subject and FA and connectivity measures were plotted in everey voxel which is probably part of this major fibre tract. For this reason a seed region (as part of the internal capsule) and target

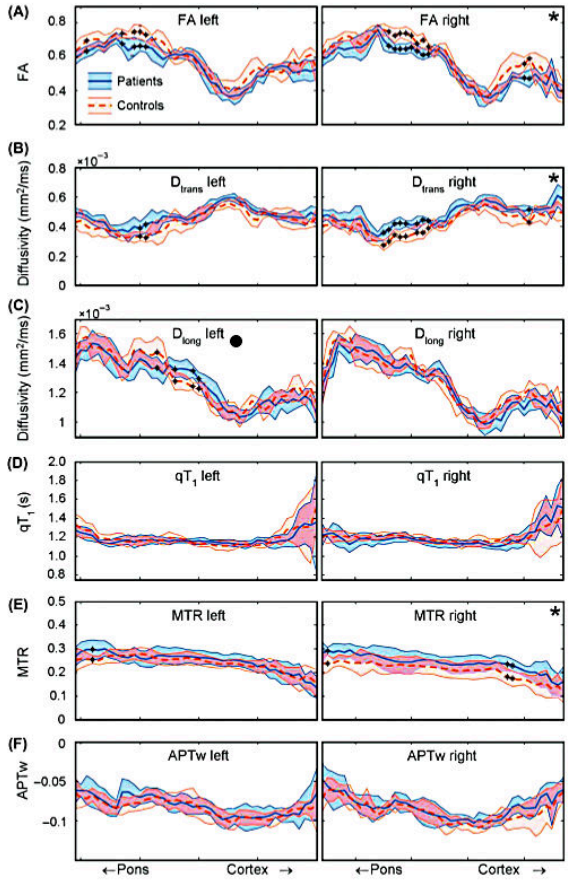

Figure 2.4: Image taken from [72] - showing the different MR contrasts along the CST (The median values and interquartile ranges are shown). An asterix in the right top of the graph indicates a significant change. Patients are marked in blue, controls are red (A) FA was significantly lower in patients in the right CST (B) The longitudinal diffusivity D_{trans} showed significant higher values in patients, (C) the longitudinal diffusivity showed no difference, (D) quantitative T_1 mapping also showed no significant changes (E) MTR is significantly increased in Patients along the right CST, (F) APTw showed no significant changes

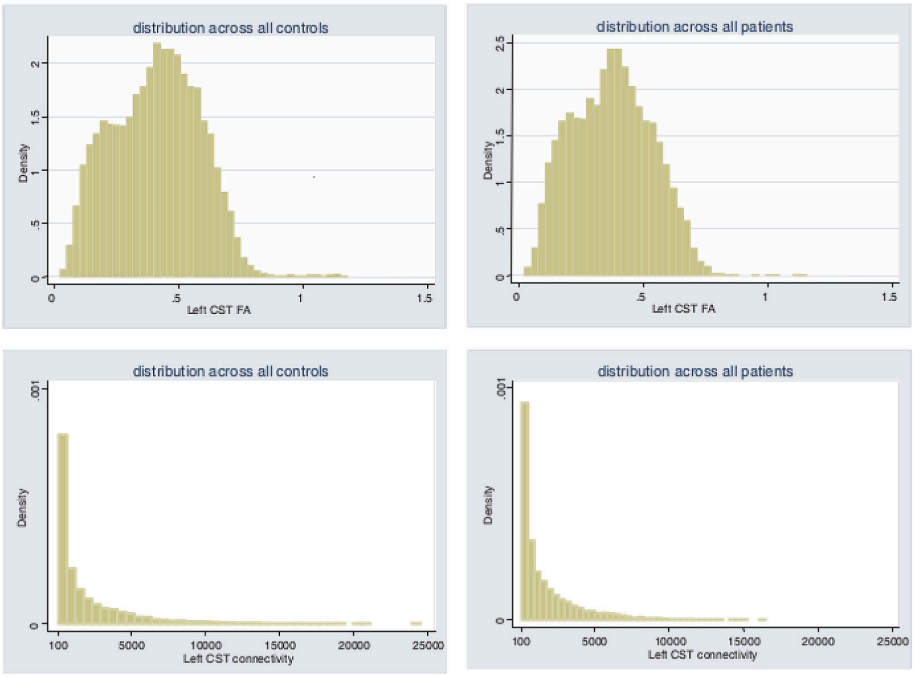

Figure 2.5: Distributions of FA values and connectivity measures sampled along the CSD. Connectivity measures were thresholded at 100, further analysis was done to the right tail of the distribution (values over 75th centile - top quarter connectivity)

regions on the primary motor cortex were defined. Then the streamlines which pass from each voxel of the seed region to the target region were counted. The resulting connectivity map (of the seed region) was thresholded to include only voxel with a connectivity value above 100. The binarized version of this map was then used as mask for the FA-map (So the FA was only plotted if the connectivity measure to the CST was high enough). Histograms of FA and connectivity measures of all subjects were drawn to show the distribution across all patients and controls (see figure 2.5). These histograms were analysed by taking only values above the 75th centile (top quarter mean connectvity) and by averaging all values. Statistical analyis was done on 3 groups whereas the patient group was subdivided in patients with *moderate disease progression* (all subjects with a progression rate below the median) and *rapid disease progression* (progression above the median). They found no significant difference between the whole group of ALS patients and controls in the mean connectivity values in both CST but a borderline significantly lower

mean connectivity in patients with rapid progression in the left CST ($p = 0.08$). Patients with moderate disease progression showed no significant difference in mean connectivity. When looking at the number of voxels containing top quarter connectivity measures patients with rapid disease progression had a lower proportion (in relation to the number of voxels identified as CST) than controls. Again patients with moderate disease progression showed no significant difference. Differences in Fractional Anisotropy were found both in the left and right CST for ALS patients. Identical results were found by regarding only the top quarter mean FA values. One of the most interesting result is certainly the correlation of disease progression with both top quarter mean connectivity and top quarter mean FA in the left CST.

The fact that they excluded the brain stem from the CST was discussed as possible weaknesses of their study. They conclude that anisotropy and connectivity can give complementary information, as one can detect pathological changes in all patients or might be used as a marker of disease progression rate.

Mapping of Iron Deposition in Conjunction With Assessment of Nerve Fiber Tract Integrity in Amyotrophic Lateral Sclerosis - Langkammer et. al. - 2010 [51]

The aim of this study was to test whether there is an increased accumulation of iron in brains of ALS patients. The methods used include *quantitative mapping of iron deposition* with R_2^*-maps, *DTI* and *tract based spatial statistics (TBSS)*

Fifteen patients and the same number of healthy controls (age- and gender matched) underwent MRI at 3T to acquire a T_1, gradient echo images with different echo times to map R_2^* and diffusion weighted data (12 independent directions, $b = 1000$ s/mm^2).

The calculation of the Diffusion Tensor and the preprocessing (eddy current correction, skull extraction) was done with FSL. TBSS was used to study diffusion characteristics. FA and *Mean Diffusivity* (MD) were calculated from DT data. For further analysis the deep gray matter of the brain was subdivided into different structures containing the

nucleus accumbens, amygdala, caudate nucleus, hippocampus, globus pallidus, putamen and thalamus.

When studying the former calculated maps (R_2^*, FA and MD) an increase of R_2^* in patients was exclusively found in the *caudate nucleus* indicating a higher iron content in this area. The regional FA was significantly lower in patients in the *globus pallidus* and the *putamen*. Regional anlysis in the later region revealed an increased MD in patients compared to healthy controls.

Regional analysis of R_2^*, FA and MD along the segmented corticospinal tract did not show differences, however the TBSS analysis of the DTI data demonstrated a significantly reduced FA in the mesencephalic part of the CST in ALS patients. The R_2^* maps indicated that iron levels in adjacent regions of the CST were increased whereas the changes were more pronounced in the left than in the right CST.

As the regions of increased iron content did not exactly match the regions with reduced FA and increased MD they discussed the possible presence of independent neurodegenerative processes. Another important point they mentioned is that an increased R_2^* value could also reflect microstructural tissue changes and not necessarily suggest changes in iron content.

Summary and additional studies

Although studies revealed contrary results, nearly all of them observed a decreased fractional anisotropy ([71],[72],[15],[17],[51],[2]), which certainly is an indicator of a change in the microstructural organization of fibre tracts. In most of the cases the affected regions coincided with the motor areas of the brain, including the corticospinaltract ([72],[17],[51], [2],[3]) and areas related to the primary motor cortex such as the supplementary motor area ([20],[71],[15]).

Another measure often derived from diffusion weighted data is the *mean diffusivity* which is a a scalar measure of the total diffusion within a voxel. This measure showed an increase in the CST and other motor related parts of the brain in a number of studies ([3],[2],[51]). The mean diffusivity is the average of all eigenvalues . By regarding only the highest eigenvalue one can compute the diffusivity in longitudinal direction D_{long} or contrary the

radial or transversal diffusivity D_{trans} as average of the two smaller eigenvalues of the diffusion tensor. Two of the mentioned studies ([72],[3]) also showed an increase of this measurement.

One group used *Voxel Based Morphometry* to detect differences in gray matter volumes and found that there is a decrease in patients with ALS. [20]

Another interesting difference in all of the surveys is the affected hemisphere. Most of the changes are bilaterally but higher on one side. Cossotini et al. ([20]) as well as others (e.g.: [72]) found more extensive changes in the right CST, whereas others had contrary results showing higher significances on the left side. [17],[15]

To summarize, it is known that there *are* microstructural changes in a defined area of the brain affecting several measures derived from neuroimaging methods but the causes are still unknown and therefore a lot of research is still done revealing new interesting facts which may help to understand and finally enable curing this disease. For further information on ALS related studies the reader is referred to [68].

Table 2.1: Summary of methods and results of related studies

	Method	affected regions	findings
Impaired Structural Motor Connectome in Amyotrophic Lateral Sclerosis - Verstraete et. al - 2011 [71]	- dwMRI with 30 directions and 5 B_0 scans. - det. tracking - FA-weighted connectivity map - network measures: E, C, L and $Effi, S_i$ for affected subnetwork	left caudal middle frontal gyrus left precentral gyrus left pallidum left hippocampus right caudal middle frontal gyrus right precentral gyrus right paracentral lobule right posterior cingluate gyrus right precuneus cortex	∘ impaired subnetwork strongly overlaps with regions of the motor control and movement ∘ no difference in any of the graph metrics of the whole brain ∘ reduced efficiency and clustering in subnetwork
Reduced Structural Connectivity Within a Prefrontal-Motor-Subcortical Network in Amyotrophic Lateral Sclerosis - Buchanan et al. - 2014 [15]	- dwMRI with 64 directions and 7 B_0 scans, T_1 for parcellation - prob. tracking (FSLs ProbtrackX, BedpostX) - FA-weighted connectivity map - network measures: network strength S, clustering coefficient C and global efficiency E	left superior frontal left caudate nucleus left pallidum left precentral gyrus left paracentral gyrus left thalamus left posterior cingulate cortex right pallidum right precentral gyrus right paracentral gyrus	∘ impaired network consisting of 10 nodes and 12 connections ∘ no difference of graph metrics of the whole brain ∘ overlap of connections found with NBS and reduced FA areas found with TBSS ∘ all 12 connections are linked to the primary motor cortex
Multimodal tract-based analysis in ALS patients at 7T: A specific white matter profile - Verstraete et al.- 2014 [72]	- DTI: FA, $D_{\text{trans}}, D_{\text{long}}$, q$T_1$, MTR, APTw - histograms of MR contrasts - averaged MR contrast along CST	right corticospinal tract	∘ decreased FA ∘ increased magnetic transfer ratio (MTR) and D_{trans} ∘ increase of free liquid spins pointing in the direction of tissue changes such as proliferation of glial cells and extracellular matrix expansion [72]
Probabilistic diffusion tractography: A potential tool to assess the rate of disease progression in amyotrophic lateral sclerosis - Ciccarelli et al. - 2006 [17]	- dwMRI with 54 directions and 6 B_0 images as well as 6 low $b-$valued images - prob. tracking - connectivity and FA values along the CST	CST bilaterally left CST left CST	∘ reduced FA ∘ lower top quarter mean connectivity in patients with rapid disease proegression ∘ disease progression correlated with top quarter mean connectivity and top quarter Fractional anisotropy in the left CST ∘ no difference in mean connectivity between controls and patients
Mapping of Iron Deposition in Conjunction With Assessment of Nerve Fiber Tract Integrity in Amyotrophic Lateral Sclerosis - Langkammer et al. - 2010 [51]	- dwMRI with 12 directions and 1 B_0 image - DTI: FA and MD - R_2^* maps - TBSS and regional analysis along the CST	caudate nucleus putamen, pallidum putamen mesencephalic part of the CST	∘ increased R_2^* ∘ decreased FA ∘ increased MD ∘ TBSS analysis showed increased R_2^* as well as decreased FA.

	Method	affected regions	findings
Structural and functional evaluation of cortical motor areas in Amyotrophic Lateral Sclerosis - Cosottini et al. - 2012 [20]	- 3D T_1 weighted on 1.5T - differences in grey matter analyzed with Voxel-Based Morphometry (VBM) - fMRI	precentral gyrus postcentral gyrus superior/middle and inferior frontal gyri SMA (supplementary motor areal) supperior/inferior parietal cortices **bilateral, but more extensive on the right side**	∘ reduced clusters of cortical grey matter in ALS patients
Voxel-Based Morphometry Study of Brain - Volumetry and Diffusivity in Amyotrophic Lateral Sclerosis Patients With Mild Disability - Agosta et al. - 2007 [2]	- T_1, T_2 - dwMRI (12 directions, $b = 900$ mm/s^2) - DTI measures: FA, MD	right precentral gyrus right superior temporal gyrus left inferior frontal gyrus left superior temporal gyrus	∘ reduced grey matter
	- Voxel Based Morphometry (VBM)	right corpus callosum (splenium) right inferior frontal gyrus right superior temporal gyrus left/right middle temporal gyrus left lingual gyrus	∘ increased mean diffusivity
		left/right corticospinal tract (midbrain) left/right corpus callosum	∘ decreased FA
Assessment of White Matter Tract Damage in Patients with Amyotrophic Lateral Sclerosis: A Diffusion Tensor MR Imaging Tractography Study - Agosta et. al - 2010 [3]	- T_1,T_2 - dwMRI - DTI measures: FA, MD, $D_{\text{long}}, D_{\text{trans}}$ - tracking of major fibre tracts → white matter probability maps → thresholding at 40 % → masks for DTI measures → average along the tracts	CST bilaterally right uncinate fasciculus	∘ increased MD and D_{trans} ∘ FA sign. correlated with disease progression ∘ increased D_{long} ∘ T_2 hyperintensities in 54% of the ALS patients

3 Methods

3.1 Participants and MRI acquisition

MRI acquisition Structural images were acquired with an MPRAGE sequence with a resolution of 1mm isotropic (TR/TE/TI/FA = 1.9s/2.19ms/0.9s/9°).
DwI data were collected using a two-dimensional diffusion weighted EPI sequence with 12 collinear directions (TR/TE/FA = 6.7s/95ms/90°) and an image resolution of 2x2x3mm^3. The $b-$value was set to 1000 mm/s^2 and 4 averages as well as 4 images with no gradient weighting (B_0) were acquired.

Participants Thirty-one patients with definite or probable ALS according to El Esorical criteria [14] (mean age ± SD: 58.1 ± 13.0 years, range: $32-82$ years, 12 female) and thirty-four healthy controls (mean age ± SD: 57.5 ± 13.2 years, range: $29-80$ years, 11 female) underwent both a T_1-weighted scan and a diffusion weighted scan at 3T. Their functional impairement was rated with the *Amyotrophic Lateral Sclerosis Functional Rating Scale-Revised* (ALSFRS-R). [13] The mean ALSFRS-R was 31.6 ± 8.4 (range: $9-45$). The mean disease duration T_{disease} was 22.0 ± 20.7 months with a range of $4-93$ months. The disease progression rate was calculated [51] as:

$$R_{DP} = \frac{48 - \text{ALSFRS-R}}{T_{\text{disease}}} \tag{3.1}$$

Table 3.1: Participants

	Healthy controls (n = 34) Mean ± SD (range)	**ALS patients (n = 31)** Mean ± SD (range)
Age (years)	57.5 ± 13.2 $(29 - 80)$	58.1 ± 13.0 $(32 - 82)$
Sex (male/female)	23/11	19/12
Disease duration (months)		22.0 ± 20.7 $(4 - 93)$
ALSFRS-R		31.6 ± 8.4 $(9 - 45)$
Progression (per month)		0.78 ± 0.85 $(0.27 - 4.17)$

SD = Standard Derivation

with a mean R_{DP} of 0.78 ± 0.85 per month and a range of $0.17 - 4.17$ per month.

3.2 Determining structural connectivity

This chapter describes the seperate steps in connectome processing in detail. Structural connectivity is calculated by a probabilistic approach. [11] The regions which define the connectivity were parcellated on T_1-weighted images. [31]

3.2.1 Overview

To generate a connectome two different types of MR images are needed: a morpholigical scan (typically a T_1-weighted scan) and a diffusion scan which are processed as separate streams. The final connectome can be obtained by registring and merging the data from the two streams. The schematic of such a pipeline is shown in figure 3.1.

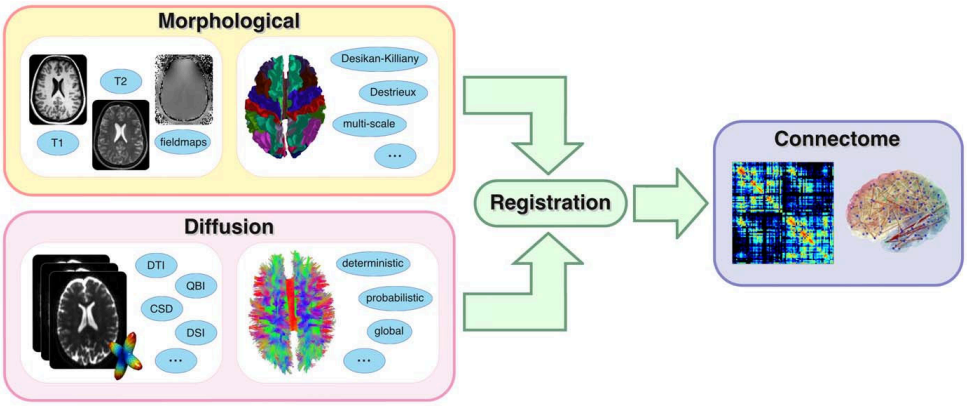

Figure 3.1: An overview of the connectome pipeline taken from [22]

Segmentation and parcellation The anatomical scan was used to generate the *nodes* of the connectome network. Therefore the brain is extracted from the skull and segmented into subcortical and cortical areas (gray matter, white matter, brain stem, ...). Both segmenation and surface extraction were done with *Freesurfer*'s `recon-all` command which is described in detail in section 3.2.1.1 **Segmentation**.

The next step is called *parcellation* and describes the division of the cortex into distinct regions of interests. These regions define the *nodes* of the brain network and are also used as seed points for fibertracking. These steps are described more precisely in the following section 3.2.1.1 **Parcellation**.

Determining Connectivity Additionally a connectivity measure is needed: In the case of a structural connectomics this measure is derived from the fiber tracts which connect two regions (nodes).

As described in chapter 2, the main fiber tracts can be modeled with methods on diffusion-weigthed MR images: After motion- and eddy-current correction the dwMR images are used to generate a *diffusion/fiber orientation function* in each voxel so that one can model the preferred direction of water. The generation of this *fiber orientation function* depends on the model of diffusion which is used - here a *Bayesian estimation of diffusion parameters*

was used. Many samples of probable directions of diffusion are generated to build an empirical estimate of the distribution of diffusion parameters. The diffusion parameters are the two spherical angles θ and ϕ, which define the direction of axonal diffusion and a diffusivity d which describes the isotropic diffusion in each voxel. Further details of the method can be found in 3.2.1.2.
After the estimation of diffusion parameters, one can tract fibers by following the preferred diffusion direction at each voxel starting and ending in defined regions (which were defined in the morphological stream before.) This procedure is also done with a probabilistic approach. A high number of possible streamlines is generated for each region and the probability of a connection is calculated by determining the fraction of streamlines which connect two nodes.

Registration The fiber tracking is the point of processing where the morphological and diffusion stream meet. A registration has to be done to combine these two different image types and to generate the final connectivity matrix. Both the anatomical and the diffusion scan were processed sequentially for every subject, thus a linear registration was used here.
The parcellated brain defines the nodes of the network and the probabilistic measure of connectivity was used to calculate the matrix. A network matrix is generated for every single subject, showing the probability of each region to be connected to others.

As might be expected there is not only one ideal solution for each of these steps and there exists no *gold standard* one can refer to. The methods used in this thesis are widely used in recent studies and were selected because they are robust and can handle the given data. Although tested, other methods are not described in this thesis.

3.2.1.1 Morphological stream

The anatomical scan was used to parcellate the brain into different anatomical regions of interest. The first step in this process was the segmentation and surface extraction.

Segmentation and Surface Extraction Segmentation and Surface Extraction was done with *Freesurfer*[1] using the command `recon-all`. This tool runs a whole suite of different commands. The methods used in this step are described in the following section.

The method: *Automated Labeling of Neuroanatomical Structures in the Human Brain*

1. The T1-weighted image of every subject is normalized to correct non-uniformities in MR data.

2. An affine transform to the Talairach atlas is computed.

> *Brain Atlases:*
>
> A brain atlas is a 3D coordinate space which maps individual coordinates to the (known) location of brain structures independent from individual differences like shape or size. For this reason the correlation between the individual volume and an average volume composed of a large number of previously aligned brains is maximised by a gradient descent algorithm at multiple scales. [28]

3. As a next step the brain is extracted from the skull. Therefore non-brain tissue is removed with a hybrid watershed/surface deformation procedure: The watershed algorithm is used to approximate the inner surface of the brain which is subsequently used as initialization for the surface deformation procedure. [40], [60]

> *Watershed algorithm:*
>
> This method interprets image intensities as height information: the brightest points correspond

[1] http://freesurfer.net/

to hills whereas the darkest points represent the valleys. With this interpretation the image can be segmented into different basins, following the ridges of this virtual landscape. [60]

In a T_1-weighted image white matter is connected and surrounded by the „darker“ gray matter and „even darker“ CSF. As the watershed algorithm segments the „valleys“ and not the „hills“ the images are inverted in a preprocessing step so that the white matter and the gray matter build up „the valley“ and are fully segmented from the CSF and the skull.
This segmentation serves as initialization for an active contour algorithm.

Active contour models

...where introduced by Kaas in 1988 [49] and are premised on the fact that an initial active contour $\mathbf{S}_0$ can be iteratively changed by a force $\mathbf{F}$ to create the desired shape. Mathematically expressed:

$$\forall p \in P \quad \mathbf{S}(p,0) = \mathbf{S}_0(p) \tag{3.2}$$

$$\forall (p,t) \in P \times R^+ \qquad \frac{\partial \mathbf{S}(p,t)}{\partial t} = \mathbf{F}(\mathbf{x},t) \tag{3.3}$$

where P is the parameter space, $\mathbf{x}$ is the current location and t the actual time step. The transformation process in skull stripping is driven by three different forces: a smoothness constraint $\mathbf{F}_S(\mathbf{x},t)$, an MRI-based force $\mathbf{F}_{MRI}(\mathbf{x},t)$ which is designed to drive the template to the true boundary and an atlas based force $\mathbf{F}_A(\mathbf{x},t)$ that ensures that the surface holds shape. The evolution equation giving the coordinates $\mathbf{x}_k^{t+1}$ of the kth vertex at time $t+1$ is therefore given as:

$$\mathbf{x}_k^{t+1} = \mathbf{x}_k^t + [\mathbf{F}_S(\mathbf{x},t) + \mathbf{F}_{MRI}(\mathbf{x},t) + \mathbf{F}_A(\mathbf{x},t)]\delta t \tag{3.4}$$

With this procedure the brain can be extracted from the skull. [60], [28]

4. In order to distinguish between the different subcortical areas of the brain (i.e.: ventricle, thalamus, pallidum, putamen, cortical white matter (WM), amygdala, hippocampus,

cortical gray matter (GM), cerebral GM and cerebral WM) *automatic subcortical segmentation* is done. This procedure is based on the the method proposed of Fischl et al. in 2002. [29] It uses an Bayesian approach to construct a probabilistic atlas of the brain areas. The probability of a segmentation W given an Image $\mathbf{I}$ is according to Bayes rule:

$$p(W|\mathbf{I}) \propto p(\mathbf{I}|W)p(W) \tag{3.5}$$

where $p(W)$ is called the *prior probability* - the probability of a given segmentation W into classes c_i. It is the knowledge about the location of the brain areas by defining a probability map and manually labelling a large set of datasets into the given brain areas (= different classes). The intensity values of these different classes (e.g.: Ventricle, Thalamus) are assumed to be Gaussian distributed. Thus this prior probability (map) is called *Gaussian probability/classifier atlas*.
In contrast, the other factor $p(\mathbf{I}|W)$ is called *a posteriori probability* and is the probability of the image occurring giving a certain segmentation. By maximizing the probability of W with the given linear transformation to the atlas space $\mathbf{L}$ and the image data I, one can find the optimal segmentation W.

$$W_{opt} = \arg\max_{W} \{p(W|\mathbf{I}, \mathbf{L})\} \tag{3.6}$$

where $\mathbf{L}$ is the transformation matrix which maps the image coordinates to the atlas space. [29]

5. After segmentation, the borders between the different classes are defined. This is done by generating surfaces - the pial surface (which is the border between gray matter and CSF), the white matter surface (border between WM and GM) and the cortical surface. The main idea how to „convert“ the volume segmentation into surfaces is to find the *plane of least variance* for every voxel. For further description the reader is referred to [28] and [27].

Implementation:

All of the methods described above are done with Freesurfers' `recon_all` command. In

this process some steps have been placed with external software: The T1-weighted image of every subject was normalized to correct non-uniformities in MR data with a non-uniform intensity correction described in [62] and the command `nu_correct` from MINC (MINC software tools for neurological imaging[2]).

Brain Extraction was done with *BET* (*Brain Extraction Tool*, also part of the FSL package). [40], [60]

The methods of subcortical parcellation described above are part of the `recon_all` command (Freesurfer built-in). A selection of subcortical areas of one sagital slice is shown in figure 3.2.

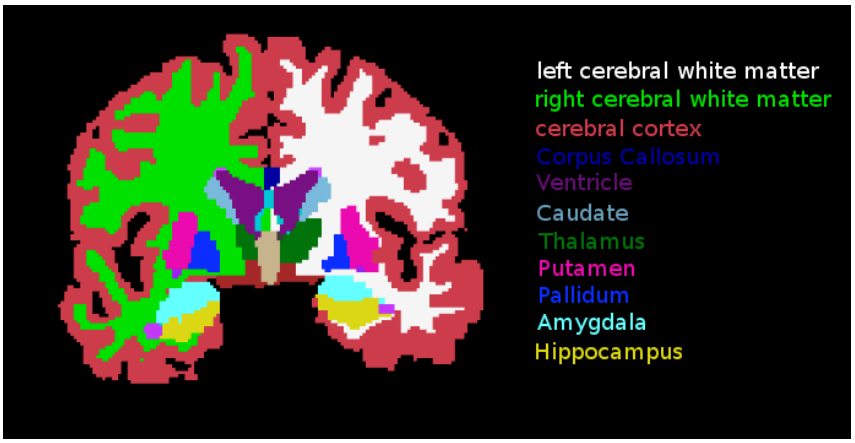

Figure 3.2: Subcortical parcellation shown for one coronal slice (selection of subcortical volumes)

Parcellation Parcellation is the process of dividing *the cortex* into different regions of interest. The technique used in this thesis is based on the method proposed of Fischl in 2004. [26]

The method: *Automatically Parcellating the Human Cerebral Cortex [30]*

Fischl presented a method for automatically assigning a neuroanatomical label to each location of the cortical surface. As it was done in the segmentation process, the parcellation is also based on a probabilistic approach incorporating both geometric information

[2]http://www.bic.mni.mcgill.ca/ServicesSoftware/MINC

from the cortical model and the neuroanatomical convention derived from a training data set.

The problem can be stated in the bayesian framework in the same way as it was done in the segmentation process. The probability of a parcellation P given the observed surface S is therefore given as:

$$p(P|S) \propto p(S|P)p(P) \tag{3.7}$$

With this approach one can include a prior information via $p(P)$ and the conditional probability of observing the surface S given the classification $p(S|P)$. These probabilities can also be defined in an atlas space with the advantage that its coordinates have more anatomical meaning compared with the native coordinate system of an image. [28] The link between the native coordinates and the atlas coordinates $\mathbf{r}$ is the atlas function f. Therefore the native coordinates can be expressed as $f(\mathbf{r})$

The question which remains is how the prior information of the parcellation can be accessed: In this method it is done by a combination of learning from a training set of manually labeled cortical areas $\mathbf{c}_i$ and a probabilistic atlas based on a large number of subjects. In the manually labeled training set the probability of a parcellation label c occuring at each atlas location $p(P(\mathbf{r}) = c)$ is computed by counting the times that class c occured at location $f(\mathbf{r})$ independent from all other classes. To get more spatial information also pairwise probabilites are computed for every possible combination of classes (e.g.: fusiform can never be a neighbour of precentral). This prior information available, the problem statement in 3.7 can be solved.

In the following the surface S of equation 3.7 at each point $f(\mathbf{r})$ is summarized by two quantities encoded as a vector $\mathbf{G}(f(\mathbf{r}))$. With the known atlas function f equation 3.7 can be written as:

$$p(P|\mathbf{G}, f) \propto p(\mathbf{G}|P, f)p(P) \tag{3.8}$$

By assuming that the noise at each vertex is independent from all other vertices on the surface the conditional probability of all classes **c** can be written as:

$$p(\mathbf{G}|P, f) = \prod_{\mathbf{r}\in S} p(\mathbf{G}(f(\mathbf{r}))|P(\mathbf{r})) \tag{3.9}$$

Also, the prior probability of the full parcellation is extended to:

$$p(P) \propto \prod_{r\in S} p(P(\mathbf{r})) \prod_{i=1}^{K} p(P(\mathbf{r})|P(\mathbf{r}_i), \mathbf{r}_i) \tag{3.10}$$

where K is the number of vertices on S. With eq. 3.9 and 3.10 the formally stated problem is nothing more than computing the parcellation $P(\mathbf{r})$ that maximizes the conditional posterior probability.

$$\begin{aligned} P(\mathbf{r}) &= \arg\max_c p(P(\mathbf{r}) = c|P(\mathbf{r}_i), \mathbf{G}(f(\mathbf{r})), \mathbf{r}_i) \\ &= p(\mathbf{G}(f(\mathbf{r}))|P(\mathbf{r}) = c = p(P(\mathbf{r}) = c) \sum_{i=1}^{K} p(P\mathbf{r}_i)|P(\mathbf{r} = c, \mathbf{r}_i) \end{aligned} \tag{3.11}$$

Eq. 3.11 is iteratively applied until convergence.

The atlas used in this thesis was proposed of Desikan et al. in 2006 [24] and is therefore called *Desikan-Kiliany* atlas. It is composed of 34 areas for each hemisphere. With a training set of 40 manually labeled T_1 MRI scans the method described above was used to automatically segment the given cortical surface on the inflated cortices. (An example of an inflated parcellated cortex can be seen in figure 3.3 (b)).

Implementation:

Parcellation is also part of the `recon_all` command. `mris_ca_label` is called to generate the parcellated brain surface. The resultant files are saved seperately for the right and left hemisphere and are called `rh/lh.aparc.annot`. The subcortical areas and the regions of the cortical parcellation yields 83 distinct regions (A listing is given in the appendix in table 5.1). An example of a parcellated brain is shown in figure 3.3

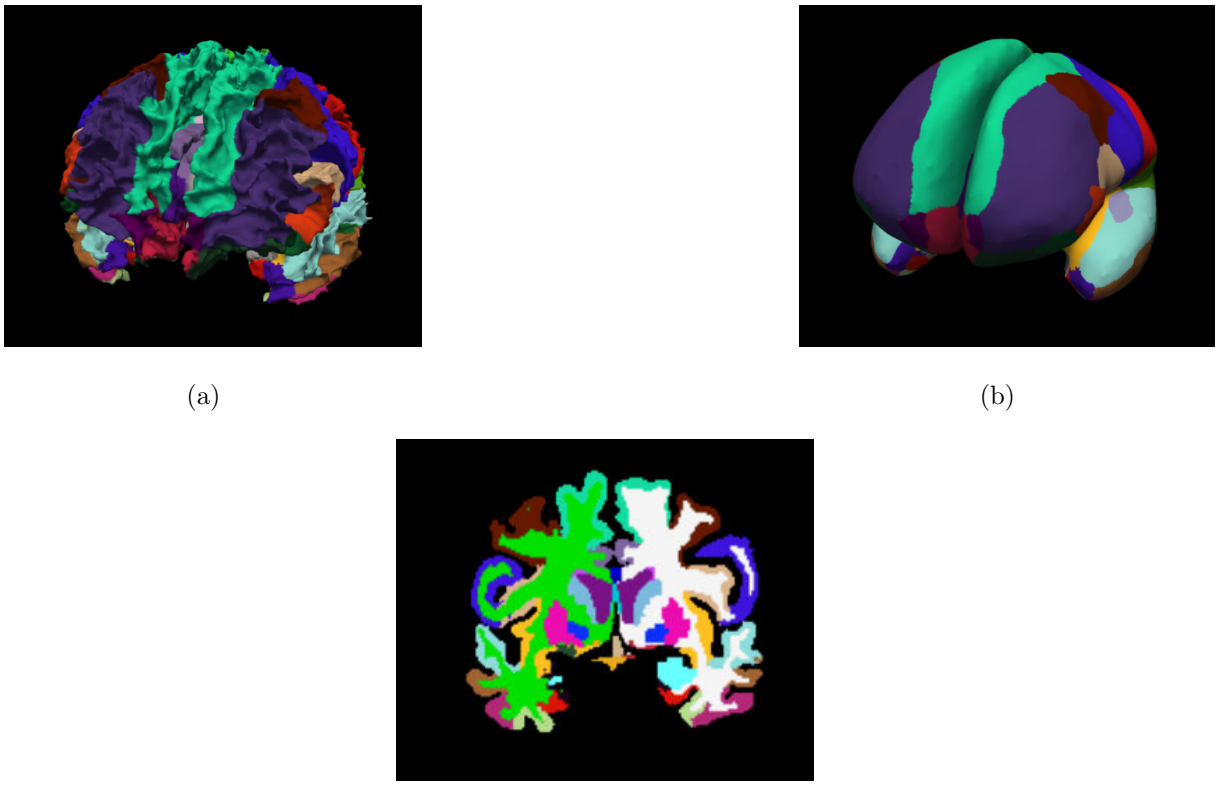

(a) (b)

(c)

Figure 3.3: Fully parcellated brain mapped to (a) white matter surface (b) inflated (c) volume (colorcodes can be found in table 5.1 in the appendix)

Registration Registration is the process of transforming different sets of data to one common coordinate system. Since there are two different image acquisition schemes (T_1 and dwI) the data has to be registered.

The method: *FLIRT of FSL*

FLIRT stands for *FMRIB's Linear Image Registration Tool* and is part of the FSL package [3]). Linear registration includes rotation, scaling, translation and shearing. The aim of linear registration is therefore to find the *best* set of parameters (rotation, scaling shearing,...) to map one image to a selected target.

To find the best set of parameters FLIRT uses a global optimization procedure in several

[3]http://fsl.fmrib.ox.ac.uk/fsl/fslwiki/

resolution levels ($n = 8, 4, 2$ mm) with 12 degrees of freedom (affine transform). The optimization procedure is based on minimizing a given cost-function. This cost function should present the difference/similarity in the two images. Several measurement of similarity exist as a basis for cost-function - depending on what type of images are need to be registered. Common measurement are the

- *Least squares of the image intensities* (same modality,contrast,subject)
- *Normalized correlation* (same modality,contrast,subject)
- *Correlation ratio* (same subject, different contrast and modality)
- *Mutual information* (same subject, different contrast and modality)

Images acquired from different subjects other registration methods such as non-linear registration. [46],[47]

Implementation:

The reference space used here was the first diffusion-weighted image (which is the B_0 image), the T_1 image was registered to the B_0 image. As these two images have different resolutions the first step was to resample the B_0 image to the higher resolution of the T_1 weighted image [22]. The registration was done with the tool *FLIRT* (FMRIB's Linear Image Registration Tool) of FSL which was described above.

The *correlation ratio* was used as a marker of similarity in the two images. The target, reference and the registered image are shown in figure 3.4 [46],[47].

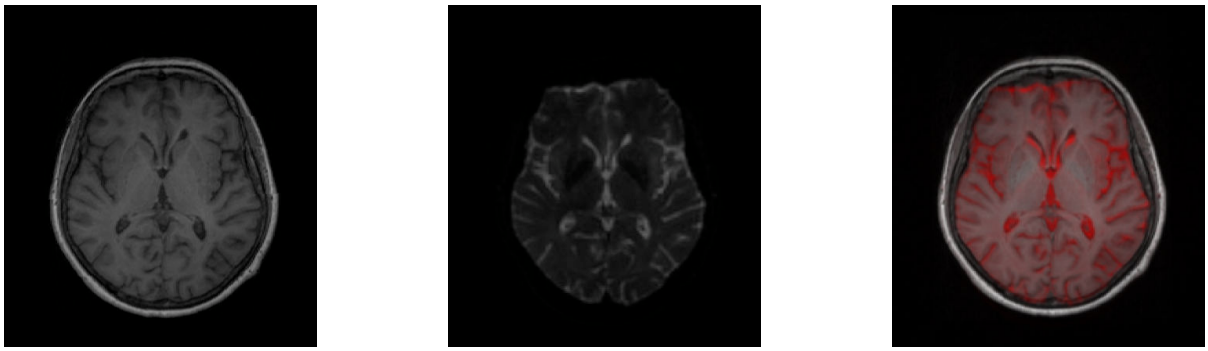

(a) (b) (c)

Figure 3.4: Registration (a) T_1 image to register, (b) target B_0, (c) resampled target and T_1, the B_0 image is colored in red and overlaid

3.2.1.2 Diffusion Scan

The diffusion weighted scan is the basis of the connectivity measurements which fill the connectome matrix. First some preprocessing is done.

Preprocessing Diffusion weighted data is acquired by adding additional gradients to the pulse sequence and therefore getting the information of the direction of free water molecules. It is assumed that there is no motion between the different gradients.
Additionally, an *eddy current correction* was done.

The method: *Linear Registration (FLIRT)*
Both motion correction and eddy current correction are done with the methods of linear registration described above (section 3.2.1.1, **Registration**)

Implementation:

Motion correction was done by registrating the diffusion gradient images to one reference image. The reference image is the B_0 image. Every other (gradient)-image had to registered to this target. The same linear registration procedure which was used to match the T_1 to the B_0 image (MCFLIRT of FSL, the MC stands for motion correction) was used. The registration was done by optimizing a cost function based on a *correlation ratio*. Every image was registered to the first one of the gradient images and as it is assumed that there is little motion between the acquisition steps, the transformation matrix of the previous image is used as initialization for the next one. [47]

Eddy current artefacts were also corrected with methods of linear affine registration. [46],[32] Figure 3.5 shows the raw and preprocessed images.

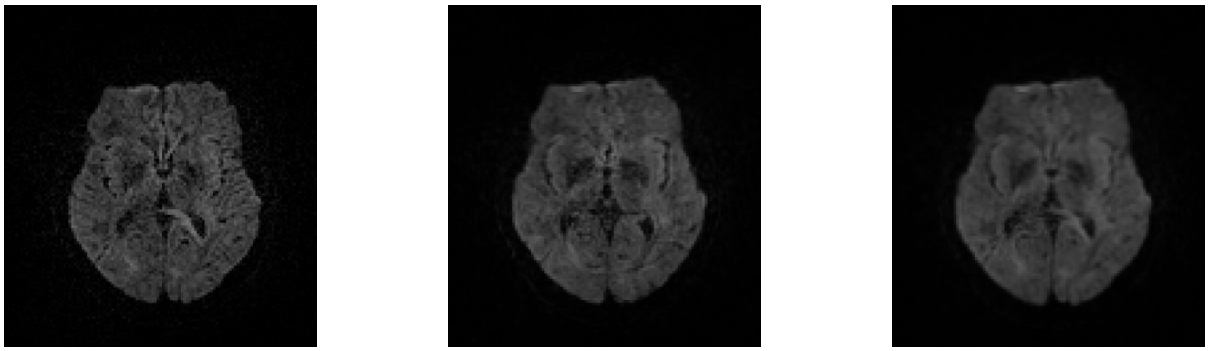

(a) (b) (c)

Figure 3.5: Same patient, same gradient number (9), same slice showing (a) raw diffusion data, (b) after motion correction, (c) eddy-current corrected image

Model of Diffusion Several models of diffusion exist (a summary is given in section 2.1.1). The method in this thesis is called *bayesian estimation of diffusion parameters obtained using sampling techniques*, in short *BEDPOSTX*, whereas the *X* stands for crossing fibers. [32]

The method: *Bayesian Estimation of Diffusion Parameters Obtained Using Sampling Techniques [11],[12]*

Model building and thus parameter estimation can be done in two ways: The most obvious one is to find the set of parameters ω which fit the data best (point estimate of the parameters). One attempt could be to find the set of parameters which *maximize* the probability of seeing this realization (= data Y) which the given model M and its parameters ω:

$$\arg\max_{\Omega} p(Y|\omega, M) \tag{3.12}$$

Another way is to associate a probability density function (pdf) of the *parameters* by *bayesian rules*:

$$p(\omega|Y, M) = \frac{p(Y|\omega, M)p(\omega|M)}{p(Y|M)} \tag{3.13}$$

This is a total different way of definition because it describes the probability of the *parameters* with the given data.

Equation (3.13) is called *posterior density*, the denumerator $P(Y|M)$ is the *joint posterior pdf* of all (possible) parameters. Both the *joint posterior pdf* as well as the *posterior pdf* are expensive to compute and often cannot be traced analytically.

Sampling techniques can be used to address this problem by drawing samples in the parameter space and reject or accept these samples according to a criterion based on the numerator in equation (3.13). The accepted samples will be distributed like the *posterior pdf* if the criteria is chosen the right way. As these methods are also computationally expensive one way is to propose samples in areas of high probability. This is called *Markov Chain MonteCarlo* technique (fig. 3.7) and can be used to draw the posterior pdf in a

relative short amount of time. [11]

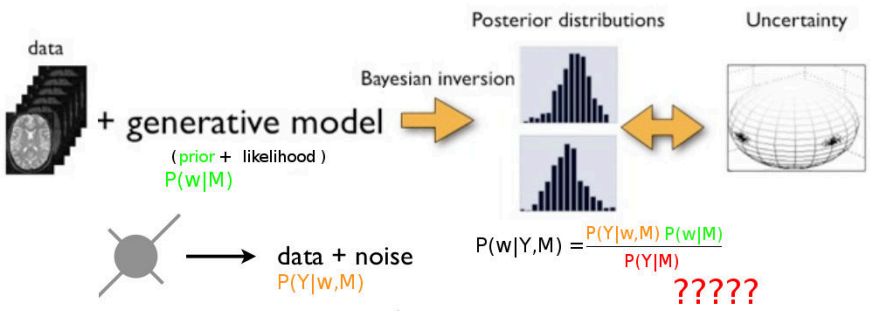

Figure 3.6: Estimation of posterior pdf, taken from [64]

The model of diffusion is a simple partial volume model, where the measured signal can be separated into an isotropic part (diffusion of free water) and an anisotropic part which models the diffusion along the fiber direction. The measured signal at every acquisition is then

$$s_i = s_0(\underbrace{(1-f)\exp(b_i d)}_{\text{isotropic}} + \underbrace{f\exp(-b_i d\mathbf{r}_i^T\mathbf{R}\mathbf{A}\mathbf{R}^T\mathbf{r}_i)}_{\text{anisotropic}}) \tag{3.14}$$

where s_i is the measured signal, s_0 the signal without gradient, f the anisotropic fraction of the signal, b_i the b-value of the i^{th} acquisition, d the diffusivity, $\mathbf{r}_i$ the gradient direction of the i^{th} acquisition and $\mathbf{R}\mathbf{A}\mathbf{R}^T$ the anisotropic diffusion tensor along (θ, ψ), with $\mathbf{A}$ fixed as:

$$\mathbf{A} = \begin{pmatrix} 1 & 0 & 0 \\ 0 & 0 & 0 \\ 0 & 0 & 0 \end{pmatrix}$$

and $\mathbf{R}$ rotates $\mathbf{A}$ to (θ, ϕ). Equation (3.14) is the model. By observing the data and some prior knowledge, we can reject or accept samples drawn in parameter space. The parameters of the ball and stick model are $(s_0, d, f, \theta, \phi, \sigma)$, where σ is the standard derivation of

the noise. It is modeled seperately for each voxel as independently identically distributed gaussian with zero mean.

For better understanding figure 3.7 should give an idea of the process in finding the *posterior pdf* of every voxel.[11]

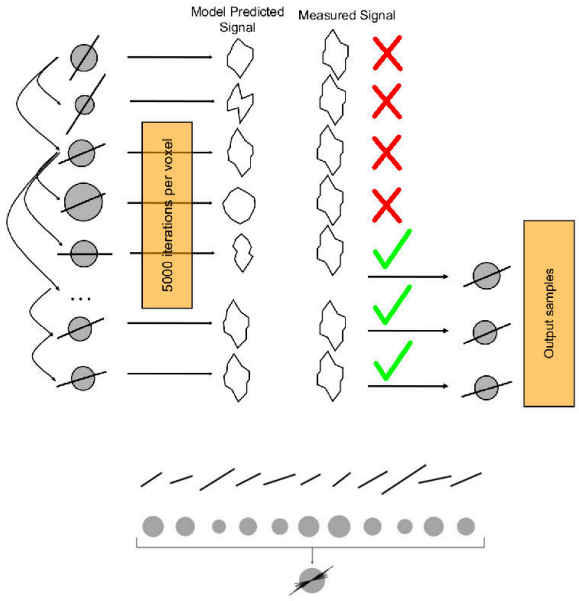

Figure 3.7: Markov Chain MonteCarlo sampling, the 1st collumn shows the samples drawn in parameter space - by comparing the predicted and the observed signal one can accept or reject this sample. If the criteria is chosen right, the accepted samples are distributed like the posterior pdf in equation (3.13), image adapted from [64], the gray balls depict the isotropic diffusion in the voxel, the black stick is the anisotropic part

This is the simplest ball and stick model and it was followed by many others. Behrens published an extension of his method 4 from 2007, [12] where *crossing* fibers can be modeled by subdividing the voxel into smaller compartements each with his „own“ anisotropic part. However, it was shown that a high number of independent gradient directions as

well as higher $b-$values are needed to get an adequate result. [12]

Implementation:

The method was implemented in the `bedpostx` command of FSL. The parameter used in this thesis were: burnin = 0 (markov chains were sampled from the beginning) with 1250 jumps where every 25^{th} jump was sampled, hence resulting in 50 samples of parameters per voxel. The number of fibers per voxel was set to 1.

The output of the *estimation of diffusion parameters* are

- 4D volumes showing the samples of the parameters θ (= th), ϕ (= ph) and the anisotropic fraction f (`merged_<th/ph/f><i>samples.nii.gz`)
- 3D volumes showing the mean of these distributions (`mean_<th/ph/f><i>samples.nii.gz`)
- 4D volume containig the main directions (`dyads_<i>.nii.gz`)

An example output is shown in figure 3.8.

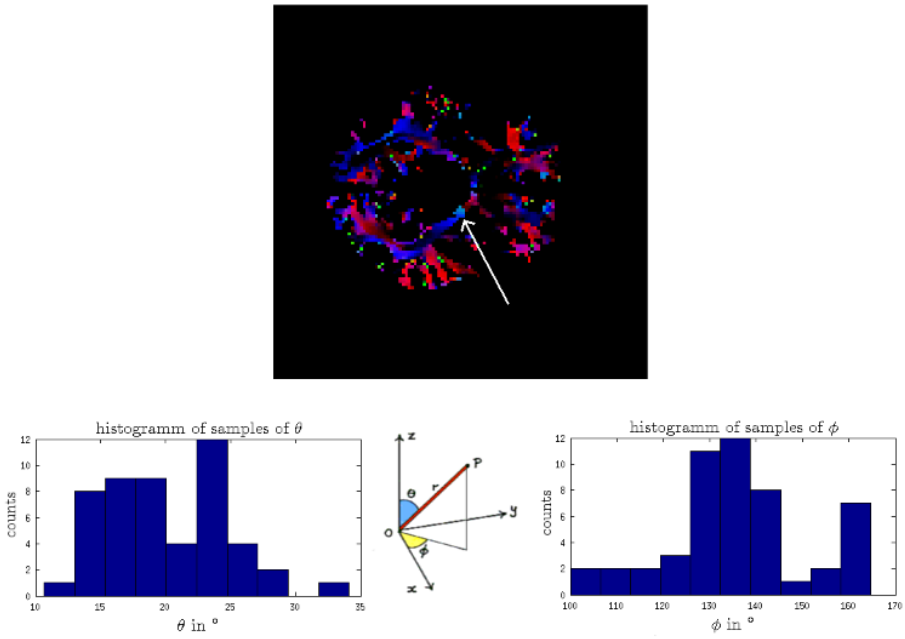

Figure 3.8: One slice showing the estimated direction of diffusion (colorcoded `dyads.nii.gz`) and the distribution of θ and ϕ in the marked voxel

Tractography

The method: *Bayesian Estimation of Diffusion Parameters Obtained Using Sampling Techniques [11] - continued*

The probability distribution function of each voxel is now used to generate a connectivity measure which characterizes the probability that region A is connected with region B, or mathematically expressed:

$$p(\exists A \rightarrow B|Y) \tag{3.15}$$

As the pdfs of the parameters do not exist in an analytical represantation but only as samples drawn in parameter space one can use exactly this representation to model the probability of (3.15). Tracking a streamline is then extremely cheap, following the given

procedure:

- The front of the streamline is the point $\mathbf{z}$
- The streamline starts at point A, $\mathbf{z} = A$
- A random sample (θ, ϕ) at $\mathbf{z}$ is selected
- z is moved a distance along (θ, ϕ)
- until a stopping criteria is met

This algorithm is repeated a given times for every region. A whole bunch of streamlines is generated. If one wants to calculate the probability that A is connected to B one simply counts the streamlines which connect A and B and divide them by the total number of generated streamlines. The main idea of this procedure is shown in figure 3.9.

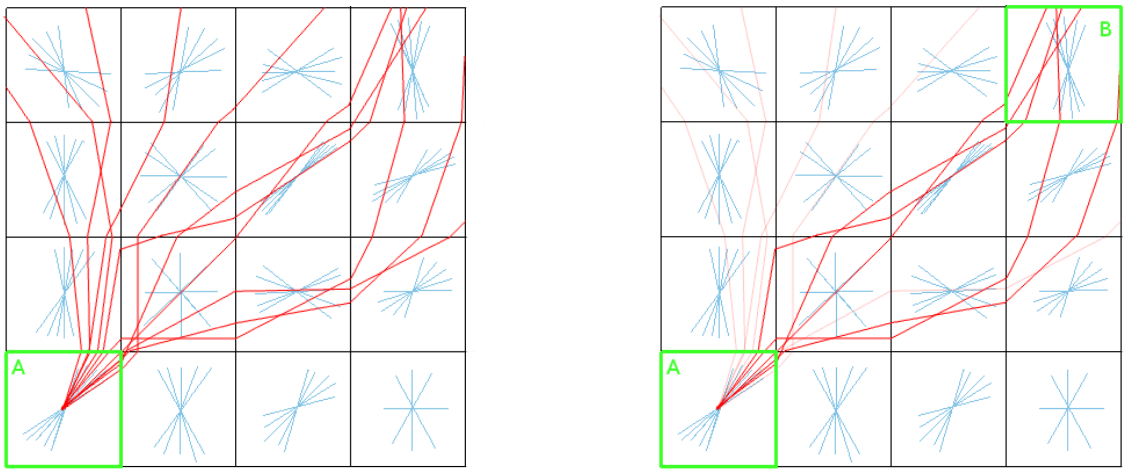

(a) (b)

Figure 3.9: 2D representation of 16 voxels with the samples of anisotropic diffusion direction, in (a) 11 streamlines were tracked seeding from region A by repeatedly choosing a diffusion direction of the given set (blue lines), in (b) only the tracts which connect A to B are shown, the probability that there is an connection between these to points is given as the number of streamlines connecting A and B divided by all streamlines, therefore $p(\exists A \rightarrow B|Y) = \frac{5}{11}$

Implementation:

The command `probtrackx`, part of the FSL package, was used for probabilistic tracking. 5000 streamlines were generated in every voxel of the given region and the curvature threshold was set to 0.2 (corresponding to a maximum angle of $\pm 80°$ otherwise the streamline was stopped here).

`probtrackx` was called 83 times (Every region defined in the parcellation before was used as a seed region, all the others were target regions). For every seed region 82 files were generated, showing the probability of the *voxels of the seed region* to be connected to one of the 82 target regions (resulting in 1 file per target region $\rightarrow$ 82 files per seed region, $83x82$ files all in all). An example of such a probability map is shown in figure 3.10.

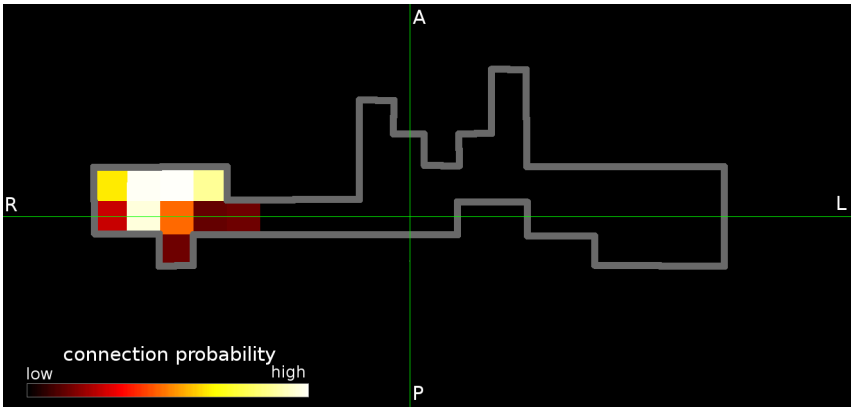

Figure 3.10: Axial slice of the brain stem (gray framed) showing the probability to be connected with the right hippocampus. As it can be seen it is more likely that the right part of the brain stem is connected with the right hippocampus, interhemispheric connections do not exist here.

3.2.2 Connectome generation

With the knowledge of the connection probability of every voxel of every region it is easy to fill the connectome matrix. This was done by summing up the probabilities of all voxels of a region resulting in the probability of the whole region to be connected to the other one. All together this results in 83x82 entries, whereas the mean diagonal is set to zero (The region cannot be connected to itself).
The final connectome is a *network* containing nodes (regions) which are interconnected by edges (connection probabilities).

3.3 Networks

This chapter will give an overview of networks in general - how they are compared to each other, how they can be visualized and a short introduction into brain networks.
A network is a mathematical model used to describe a complex system. Any networks are defined by their *nodes* and connecting *edges*.

3.3.1 Network statistics

To compare networks, one can either calculate topological measures (described in the next section 3.3.1.2) or compare the networks *as a whole* with a novel method called *Network Based Statistics*.

3.3.1.1 Network Based Statistics

The method was proposed of Zalesky in 2010 [78] with the goal to find pairwise associations which are *significantly different between groups*. The brain network generated before contains the connection probability or connectivity as pairwise association. Each subject can be assigned to a group (*case-control studies*) and for each connection probability (entry of the connectivity matrix) a groupwise statistical test is done - resulting in one matrix for all subjects showing the test-statistic for every possible link. An example of such an test-statistic map is shown in figure 4.2(a).
In the following step this *test-statistic matrix* is thresholded to find connections which are *significantly* different between the groups giving a set of *suprathresholded* connections. At this point it is important to mention that NBS is a *non-parametric method*. The thresholded test-statistic map is only the first step and used as a „preliminary decision“ - normally distributed data is not required here. [78]
When searching for differences in brain networks one is not interested in isolated, unpaired

connections - therefore the next step is to search for *connected components* in this set of suprathresholded links.

> *Connected Component*
>
> A connected component is a subset of a graph where any two nodes are connected to each other by paths. A path is a finite number of edges which connect two nodes. [53]

Any connected components are identified using a *breadth first search* and the number of links they comprise (i.e.: the *size*) of the connected component is stored.
As NBS is a non-parametric method, the individual thresholded test-statistic values are not used to determine the significance. To assign a p-value to the identified connected components permutation testing is done.

> *Permutation Testing*
>
> Permutation tests can be described as *significance tests*. These test are used to determine whether an observed effect (such as a difference of two means from two groups) could be ascribed to randomness or not. For this reason the distribution under the null-hypothesis (H_0, no difference between the groups = no effect) is studied. If an observation is somewhere located in the body of the distribution this could easily occur by chance. A value in the tail would rarely occur by chance and so this can be an evidence that something other than chance is operating. The probability, that the observed sample happened by chance, is specified with the p-value. A lower p-value indicates that there might be an effect which is caused to a lower extent by chance (= *significance*).
>
> The statement, that the effect searched for is not present in the population, is the null hypothesis H_0. *If H_0 is true it makes no difference which group a subject does belong to* (They are the same anyway). This is the principal of permutation testing. By assigning any subject a random group label (*permute* the group label) many times and observe the variable of interest again one can draw a distribution of the observed variable. If the variable observed with the „true“ assignment of the groups is much higher or lower than most of the others (somewhere in the

> tail of the distribution), it appears likely, that something other than chance is operating, the null-hypothesis can be rejected. The p-value can be calculated by counting the values of the drawn distribution which are higher than the observed one and dividing it by the total number of permutation.
>
> As an example it is assumed that out of 100 permutations only 5 values were higher than the observed variable. The probability that this happened by chance is then $\frac{5}{100} = 0.05$.
>
> The permutation distribution approximates the sampling distribution. It is non-parametric method and can be used for any distribution.

In NBS a total of M permutations are generated independently by randomly exchanging the group to which a subject belongs to. The test statistic of interest is the *size of the maximal connected component*. For each permutation the test-statistic is recalculated and thresholded in the same way as it was done before. The maximal component size of all M permutation is stored and thereby yielding an estimate of the null hypothesis of the maximal component size. The p-value can be determined easily by counting the numbers of permutations with an higher maximal component size than the observed one and normalizing by M. If the p-value does not exceed the statistical significance level a connected component is found and can be analyzed further.

Implementation:

All the calculations were done in `MATLAB` with support of the NBS-toolbox.[4] A F-Test was used to investigate any difference between ALS patients and controls. F values below 7 were discarded and significance level for NBS was set to 5%. 5000 permutations were done to assign a $p-$value to the identified connected component.

The identified subnetwork was further investigated by averaging the connectivity values of the affected subnetwork of patients and controls and by determining topological network measures. A summary of the network measures used is given in the next section.

[4] `https://sites.google.com/site/bctnet/comparison/nbs`

3.3.1.2 Network Measures

As introduced in chapter 2, a network is a „mathematical representation of a real-world complex system“ [59]. It is defined by nodes and the links between them (edges) and can be described by mathematical measures. One can distinguish between *local network measures*, which describe features of one specific node, and *global network measures*, which are used to describe the topology of the whole network. The local measures of all nodes build up a distribution, which is most commonly described by its mean.
Individual network measures normally characterize only one aspect of global or local connectivity thus the network measures are divided into measures of *density*, *segregation*, *integration* and *small-worldness*.
One can also distinguish between weighted and binary network measures. Binary network measures categorize whether there is a connection or not, whereas weighted network measures consider the weight of a link (e.g.: the probability of a connection) used in this thesis. Here we focus on *weighted network measures*. These measures are marked with an superscripted w, the subscript i marks the *local* measure of node i. No subscript indicates a *global* network measure. [59]

Measure of density The most basic network measure is the *degree* of a network. The degree of a node defines the number of neighbours and thus is equal to the number of directly connected nodes. The degrees of all nodes build up the *degree distribution*, which is an important marker of network's development and resilience. The *mean degree* describes the density of the whole network or the total wiring cost, whereas a lower mean degree depicts less density and less wiring cost. The *binary degree* k_i of a node i can be described as

$$k_i = \sum_{j \in N} a_{ij} \tag{3.16}$$

where N is the set of all nodes and n is the total number of nodes. a_{ij} is the connection status which is 1 if there exists a link between node i and j an 0 otherwise.
The *weighted degree* is given as

$$k_i^w = \sum_{j \in N} w_{ij} \tag{3.17}$$

where w_{ij} is associated with the connection weight. Weights are normalized such that $0 < w_{ij} < 1$. The weighted degree is also called *local strength* of the node. The global strength is the total sum of all weights of a network.

$$S^w = \sum_{i \in N} w_i \tag{3.18}$$

Measure of segregation *Segregation* is the ability for specialized processing in densely interconnected groups of brain regions. Such groups can be clusters or modules in this network. Simpler measures of segregation are based on the the number of triangles in the network. A high number of triangles indicates high segregation and high clustering. The number of weighted triangles around a node i is given as:

$$t_i^w = \frac{1}{2} \sum_{j,h \in N} w_{ij} w_{ih} w_{jh} \tag{3.19}$$

Then the local and global clustering coefficient $C_{(i)}^w$ and can be expressed as:

$$C_i^w = \frac{2t_i^w}{k_i(k_i - 1)} \tag{3.20}$$

$$C^w = \frac{1}{n} \sum_{i \in N} C_i^w \tag{3.21}$$

Note, that the number of triangles around the node i is normalized by $\frac{k_i(k_i-1)}{2}$ where k_i is the binary degree and not the weighted version.[59]

Measures of integration *Integration* describes the ability of rapidly combining information from distributed brain regions. These measures are commonly based on the concept of paths. A *path* is a sequence of links which connects two nodes.
The utilized measure of integration is the *characteristic path length* of a network, which is the average *shortest path length* between all possible pairs of nodes. The weighted shortest path length between nodes i and j is given as

$$d_{ij}^w = \sum_{a_{uv} \in g_{i \to j}} f(w_{uv}) \tag{3.22}$$

where $g_{i \to j}$ is the shortest weighted path from node i to j and f is a map from weight to length (in this thesis, the inverse of the weight is used as length). The mean weighted shortest path length is called *weighted characteristic path length* L^w:

$$L^w = \frac{1}{n} \sum_{i \in N} \frac{\sum_{j \in N, j \neq i} d_{ij}^w}{n-1} \tag{3.23}$$

A non-connected node has infinite path length per definition, leading to an infinite characteristic path length for the whole network. Therfore another network measure of integration can be defined: The *efficiency* is the inverse of the shortest path length. It is converging to zero if a node is disconnected, mathematically expressed:

$$E^w = \frac{1}{n} \sum_{i \in N} \frac{\sum_{j \in N, j \neq i} \left(d_{ij}^w\right)^{-1}}{n-1} \tag{3.24}$$

The local efficiency is calculated in the following way: [59]

$$E_{loc}^w = \frac{1}{2} \sum_{i \in N} \frac{\sum_{j,h \in N, j \neq i} \left(w_{ij} w_{ih} [d_{jh}^w(N_i)]^{-1}\right)^{1/3}}{k_i(k_i - 1)} \tag{3.25}$$

Measure of smallworldness A well designed network should simultaneously be able to accomplish the demands of functional integration as well as the opposing demands of segregation. It should have a high number of clusters which are efficiently connected to

each other - giving an optimal balance of functional segregation and integration. Watts and Strogatz [73] were the first ones who entitled this phenomenons: *small-world networks*. Those are formally defined as networks that are significantly more clustered than random networks but have approximately the same characteristic path length. The measure of small-worldness captures this effect by calculating the fraction of two known (normalized) measures:

$$\text{small-worldness} = \frac{\frac{C^w}{C_r^w}}{\frac{L^w}{L_r^w}} \tag{3.26}$$

where C_r and L_r are the clustering coefficient and characteristic path length of a random network with the same degree distribution and number of nodes n. A small-world network is a network with a high ($\gg$1) small-worldness. An example of a small-world network as well as the normalized characteristic path length and clustering coefficient for a different randomness is shown in figure 3.11. [59]

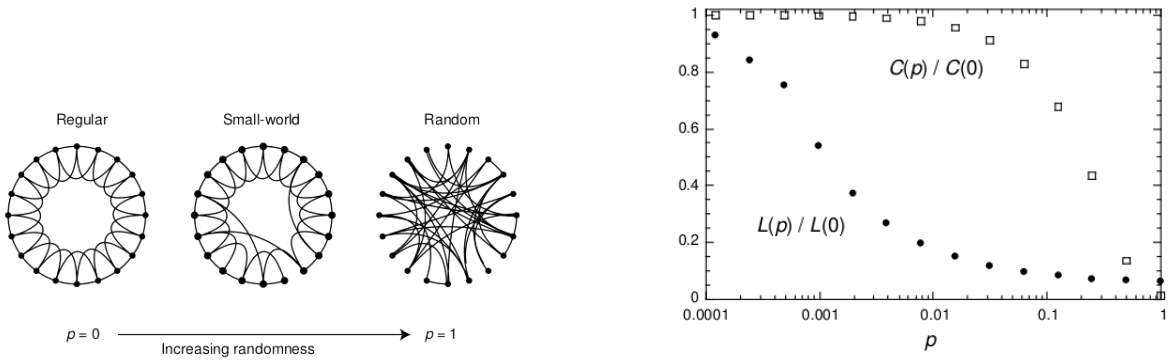

(a) (b)

Figure 3.11: Small-world networks, (a) depicts different network types with increasing randomness, (b) shows the normalized clustering coefficient and characteristic path length for increasing randomness, both images are taken from [73].

Implementation:

The presented network measures were calculated for every subject. Calculations were done in `MATLAB` with the *Brain Connectivity Toolbox (BCT)*[5] and own Matlab scripts. The random weighted clustering coefficient C_r^w and the weighted charateristic path length L_r^w were calculated by generating 100 random networks with the same number of nodes n and the same degree distribution. The average weighted clustering coefficient and weighted characteristic path length of these 100 random networks where used estimate these random measures for every subject.

After checking for normal distributed data with the *Kolmogorov–Smirnov test* the group wise comparision was done either with a *t*-test or a *Mann-Whitney U Test* for non-normal distributed data. Significance level was set to 5%.

statistical tests for group-wise comparisions

In a *case-control study* it is important to find differences between two groups. So how are different measures compared to each other? The easiest way would be to compare the means of the cases and controls for a given contrast, but how can one be sure that the difference in means happened not just by chance? A *t*-test therefore tests whether two data sets come from the same or from different distributions by looking at their means and variances. The hypothesis to test is that the two datasets are samples of the same distribution (null hypothesis H_0, shown in the bottom of figure 3.12). By calculating the probability that this is the case (p-value), one can either reject or accept the null hypothesis. The criteria whether the null hypothesis is rejected or not is called *significance level* and is defined by thresholding the calculated $p-$value (normally $p < 0.05$ is used as significance level).

It is important to ensure that the samples of the data are normally distributed. This type of testing is also called *parametric testing* as it requires a known distribution. Another group of statistical tests is therefore called *non-parametric tests*, distribution of data does not have to be known in advance.

To ensure normality different test can be made: The most commonly used one is called *Kolmogorov–Smirnov test* which test the null hypothesis that the data *is* normally distributed.

If this is not the case *non-parametric tests* such as the *Mann-Whitney U test* can be used.

[5] available here https://sites.google.com/site/bctnet/

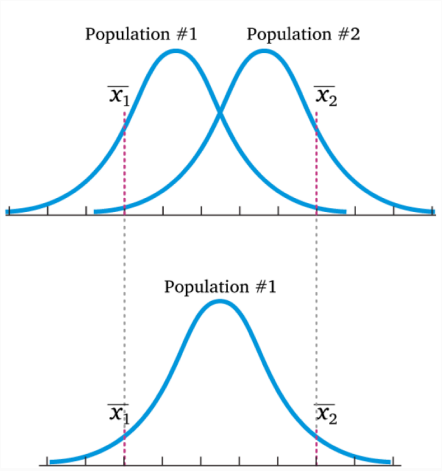

Figure 3.12: distribution and the means of two datasets, testing whether the two datasets are from the same or different distributions

3.3.2 Visualizing networks

There are several ways to visualize a network. The easiest one is certainly shown in figure 3.14 (a), where the links of every possible connection from node i to j are depicted in matrix form. The x and y axis depict the nodes of the network. Another way is to draw the nodes in anatomical space, as it was done in 3.14 (b). This is an interesting visualization for neurologists, as one can see the real anatomical locations of the nodes and any findings can be immediately characterized by their location.
Another common way of visualizing is shown in figure 3.14 (c). [43] The different regions are distributed on a circle and the connectivity probabilities are shown as lines connecting these regions. [16],[52]

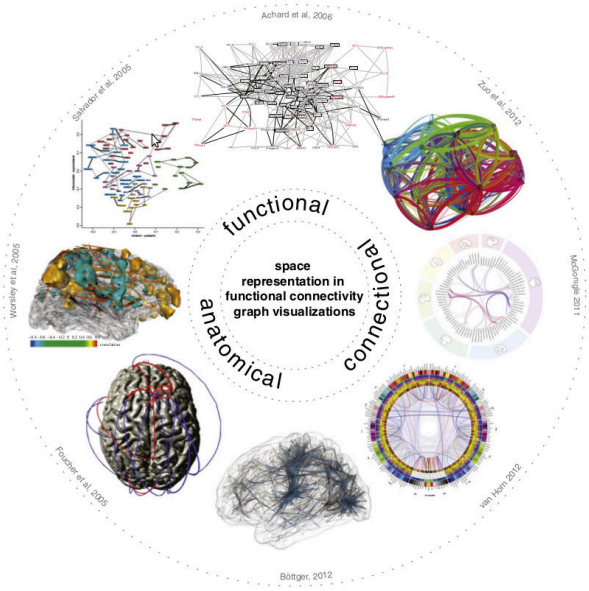

Figure 3.13: methods to represent a connectome, image taken from [52]

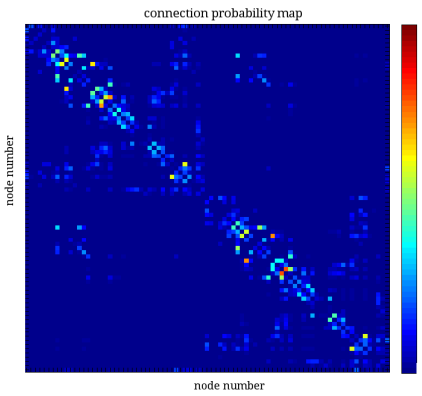

(a)

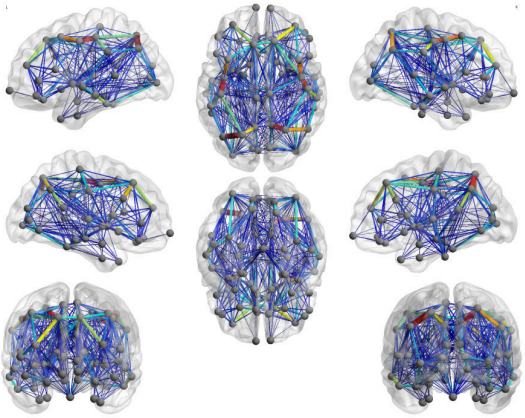

(b)

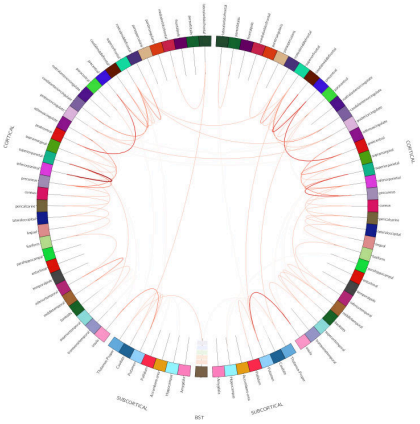

(c)

Figure 3.14: The same connection probability matrix of one patient shown in three different ways: (a) matrix where the entries in (i, j) depict the connection probability of from node i to j, (b) 3D representation of the same network, the nodes are the centroids of regions mapped to MNI - space; (c) circular representation of the same network, only edges higher than a fifth of the maximal value are shown for better illustration

Implementation:

In this thesis networks were visualized as matrices as shown in figure 3.14 (a) and as 3D - models within an anatomical space (The MNI space was used here). The visualization was done with `MATLAB` and the toolbox *BrainNetViewer*. [77]

3.3.3 Software

A number of free software for both analyzing and visualizing of brain networks or networks in general exist. A summary of the most common network toolboxes is given in table 3.2.

In this thesis the *connectomemapping toolkit*[6] was used. This pipeline includes software packages like *FSL* for brain extraction, registration, motion and eddy current correction, probabilistic estimation of diffusion parameters and probabilistic tracking, *Freesurfer* for segmentation, surface extraction and parcellation, and *MRtrix*[7] for conversion of the different data types.
Post-hoc analysis was done with *MATLAB* and the already mentioned toolboxes (*Brain Connectivity Toolbox* and *BrainNet Viewer*)

[6] `www.cmtk.org`
[7] www.brain.org.au/software/mrtrix/

Table 3.2: Available Software for Visualizing and/or Analysing Brain Networks

Package	Language	Web			Comment
ConnectomeViewer	Python	`www.cmtk.org`	√		part of the *connectomemapping-toolkit* (cmtk)
ConnectomeAnalyzer	Python	`www.cmtk.org`		√	cmtk
Connectome Workbench	C++	`www.humanconnectome.org/`	√	√	used of the *Human Connectome Project* (HCP)
BrainNetViewer	MATLAB	`www.nitrc.org/projects/bnv`	√		network can be represented in anatomical space
VisualConnectome	MATLAB	`code.google.com/p/visualconnectome/`	√	√	*SurfStat* and *Brain Connectivity Toolbox* needed
Matlabblg	MATLAB	`github.com/dgleich/matlab-bgl`		√	network algorithms
NetworkX	Python	`networkx.github.io`	√	√	High-productivity software for complex networks
Network Based Statistic Toolbox	MATLAB	`www.nitrc.org/projects/nbs`		√	special tool to compare brain networks
Brainwaver	R	`www.nitrc.org/projects/brainwaver/`		√	brain- network statistics
Circos	Perl	`circos.ca/`	√		originally used for gene networks

4 Results

4.1 Connection Probability Maps

The result of the connectome processing was basically a matrix containing the probabilities for all connections between node i and j, for every subject.
The mean connectivity measures for both patients and controls are shown in figure 4.1.

4.2 Network Based Statistics

A group-wise comparison was done for every connection in the connection probability map. A F-test, which reveals any difference in the variances of two populations, was used here.
The F-map as well as the suprathresholded links ($F > 7$) and the connected component are shown in figure 4.2. 19 nodes and 15 connections had an $F-$ statistic above 7, but only 10 connections and 11 nodes built a connected component and where further analized. A connected component is built with at least 3 nodes, connected with 2 edges. The discarded edges are isolated connections and did not build a connected component (see figure 4.2 (b)).
The maximum component size succeeded the value of 10 in 170 of 5000 permutation, yielding a p-value of 3.4% for the identified subnetwork.

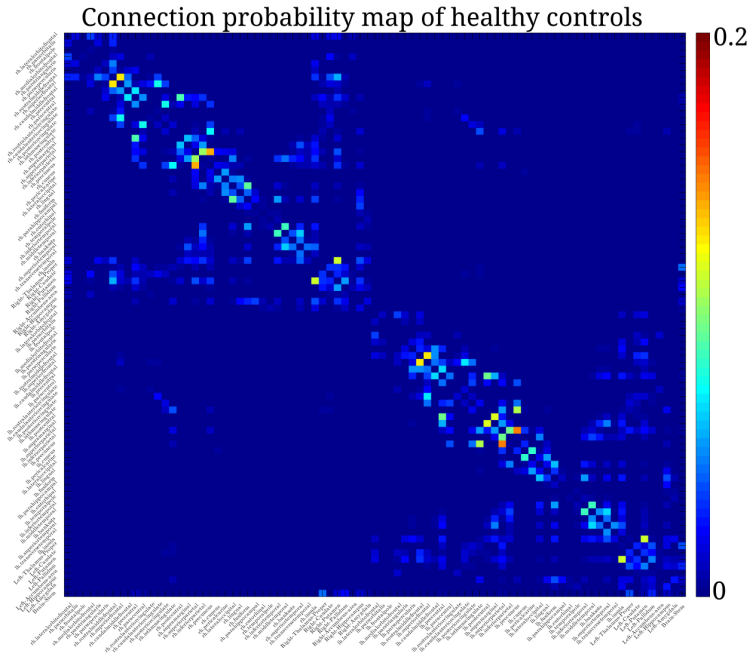

(a)

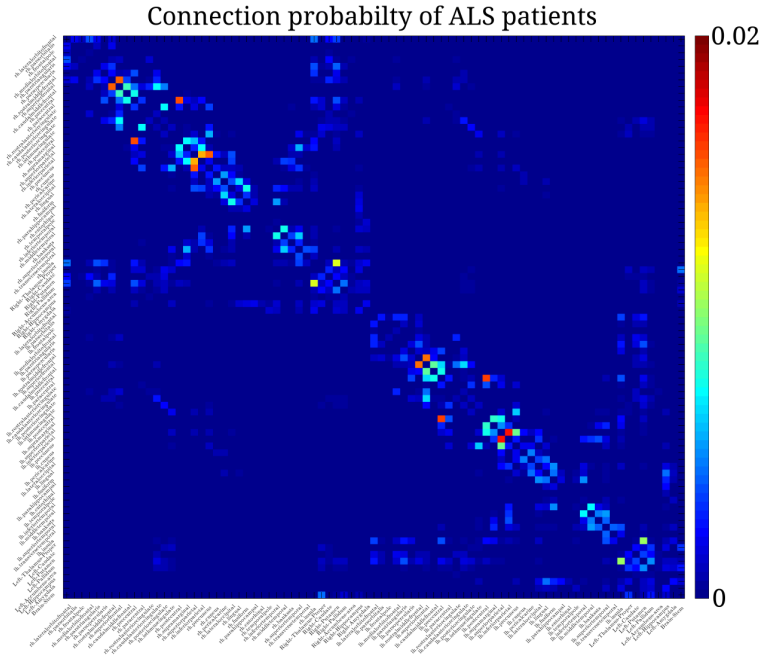

(b)

Figure 4.1: mean connection probability maps for (a) controls and (b) ALS patients; on the x- and y- axis the different regions are shown

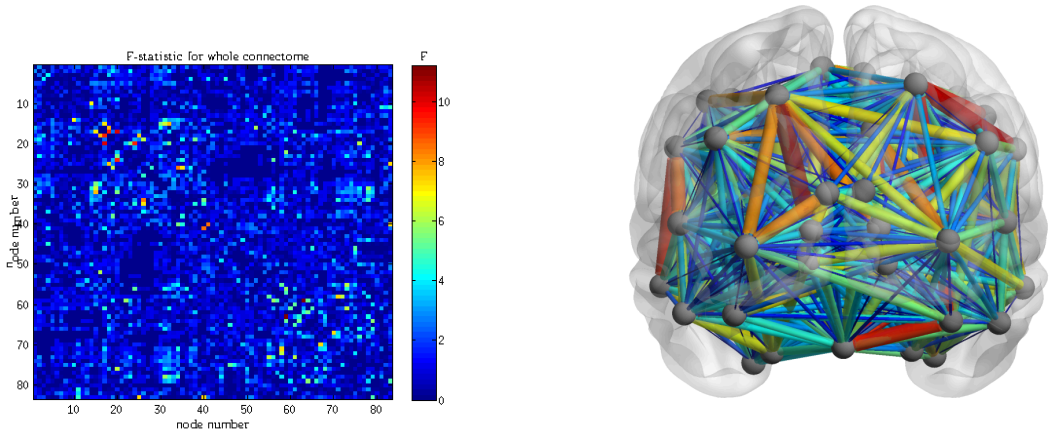

(a)

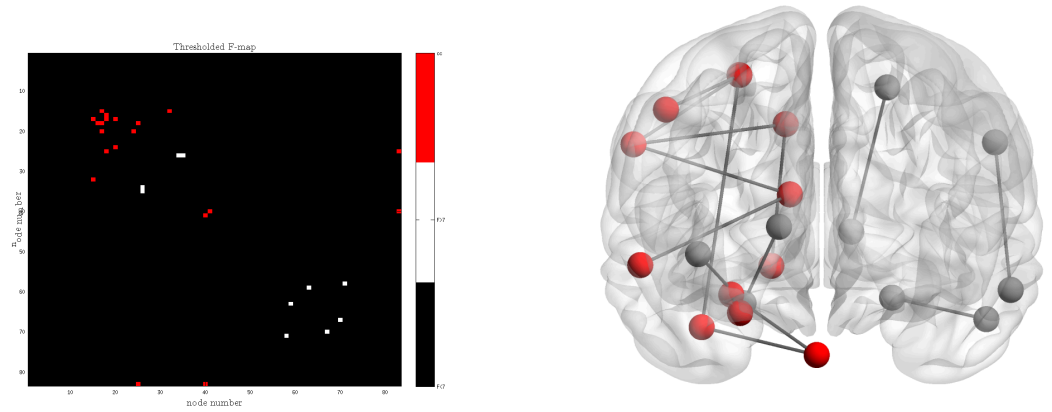

(b)

Figure 4.2: A F-test was done for every connection to test for group differences in the connectome. The corresponding F-value for every connection is shown in (a), (b) depicts the thresholded F-map whereas only the connections connecting the red nodes are kept as they form a *connected component*

Higher variance of connection probabilities in ALS patients The affected subnetwork is shown in figure 4.3.

The affected nodes (i.e.: brain regions) and the connections of the affected subnetwork are listed in table 4.1 and table 4.2:

Table 4.1: nodes of the affected subnetwork found with NBS

Number	Hemisphere	Region	Lobe	part of CST
15	right	isthmus of cingulate cortex	cingulate (parietal)	
16	right	postcentral cortex	parietal	√
17	right	supramarginal gyrus	parietal	√
18	right	superior parietal cortex	parietal	√
20	right	precuneus cortex	parietal	√
24	right	lingual gyrus	occipital	
25	right	fusiform gyrus	temporal	
32	right	superior temporal gyrus	temporal	
40	right	Hippocampus	-	
41	right	Amygdala	-	
83	-	Brain Stem	-	√

As listed in table 4.1, 5 of the 11 nodes belong to the corticospinal-tract which plays a crucial role in motor coordination, control and development.

Higher connectivity in superior parts of the brain and lower connectivity in inferior parts When considering the *means* of the connection probabilities of both patients and controls, it was found that the connection probabilities of the ALS patients are higher in the superior part of the identified subnetwork (right superior parietal cortex - right

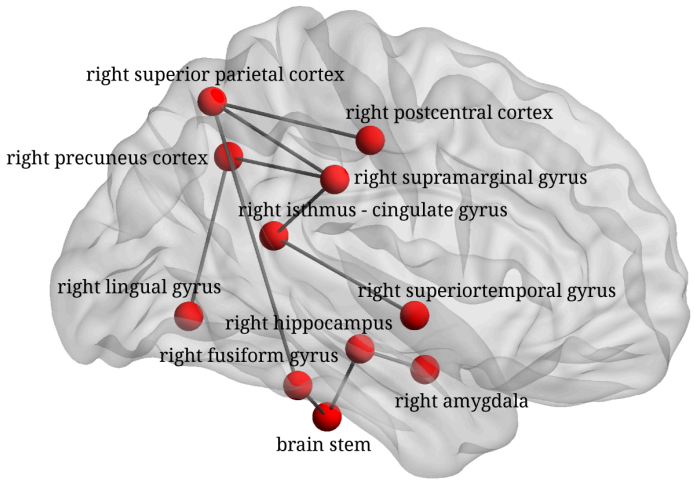

(a)

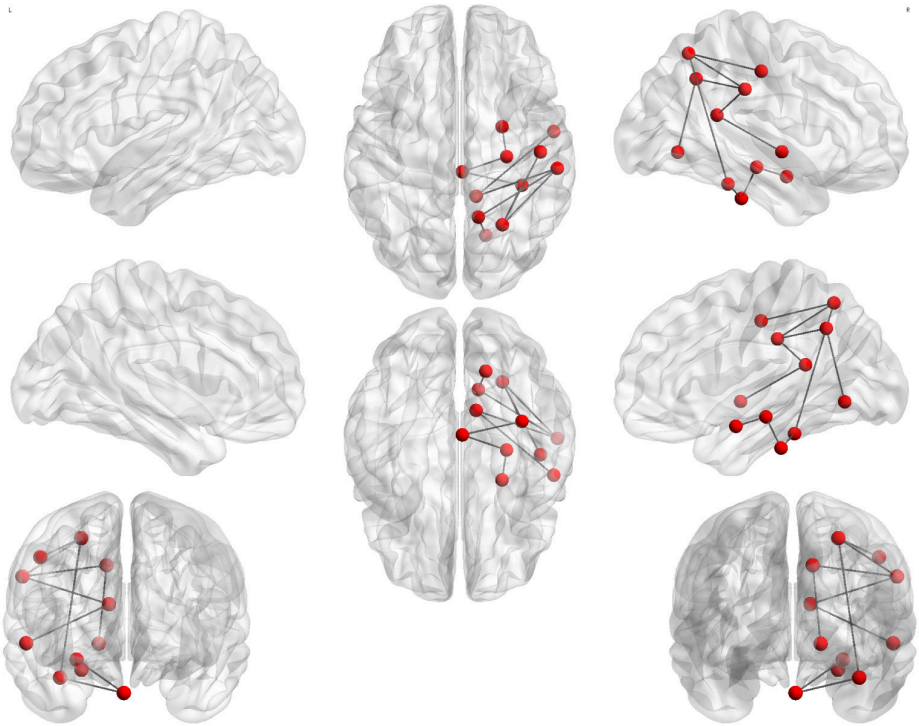

(b)

Figure 4.3: affected subnetwork showing a higher variance of connection probabilites in ALS patients

postcentral cortex; right superior parietal cortex - right supramarginal gyrus; right supramarginal gyrus - right isthmus of cingulate cortex; right supramarginal gyrus - right precuneus cortex) but lower in the inferior part of the subnetwork (right superior parietal cortex - right fusiform gyrus; right hippocampus - right amygdala; right fusiform gyrus - brain stem; right hippocampus - brain stem) as it can be seen in table 4.2.

Table 4.2: connection probabilites for ALS patients and controls in terms of mean ± standard derivation and the corresponding t and F-value

Connection	**Healthy controls** Mean ± SD	**ALS patients** Mean ± SD	t	F
right isthmus of cingulate cortex - right supramarginal gyrus	2.66e-05 ± 5.66e-05	1.18e-04 ± 1.89e-04	2.68	7.16
right postcentral gyrus - right superiorparietal lobule	3.50e-03 ± 1.13e-03	4.33e-03 ± 1.28e-03	2.76	7.59
right supramarginal gyrus - right superior parietal cortex	2.18e-03 ± 7.33e-04	2.99e-03 ± 1.32e-03	3.08	9.46
right supramarginal gyrus - right precuneus cortex	1.95e-04 ± 2.63e-04	5.05e-04 ± 4.98e-04	3.18	10.10
right precuneus cortex - right lingual gyrus	1.03e-03 ± 5.25e-04	1.46e-03 ± 6.17e-04	3.06	9.39
right superior parietal cortex - right fusiform gyrus	3.81e-04 ± 5.09e-04	1.17e-04 ± 1.81e-04	-2.73	7.48
right isthmus of cingulate cortex - right superiortemporal gyrus	7.07e-05 ± 1.27e-04	3.62e-04 ± 6.02e-04	2.76	7.61
right hippocampus - right amygdala	1.72e-03 ± 3.81e-04	1.46e-03 ± 3.34e-04	-2.91	8.44
right fusiform gyrus - brain stem	2.16e-07 ± 4.34e-07	4.87e-09 ± 1.63e-08	-2.70	7.32
right hippocampus - brain stem	1.32e-03 ± 2.75e-04	1.09e-03 ± 4.25e-04	-2.69	7.26

The difference of the *mean connection probabilities* $\mu_P - \mu_C$ of the affected subnetwork is shown in figure 4.4. Positive values indicate a *higher* connection probability in ALS patients, negative values (dark blue connections) a higher connection probability in healthy controls.

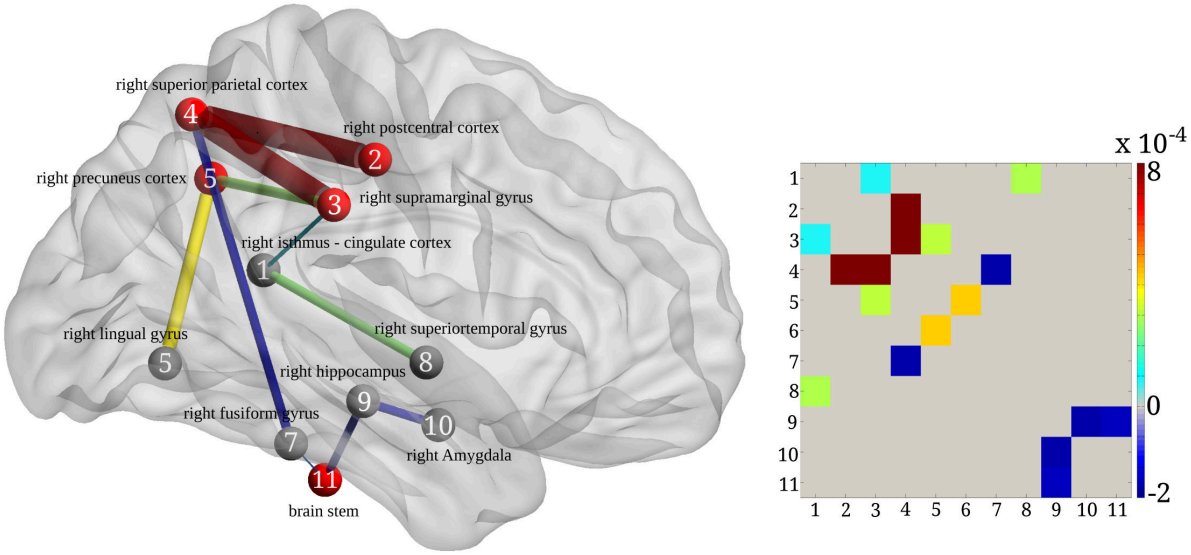

(a)

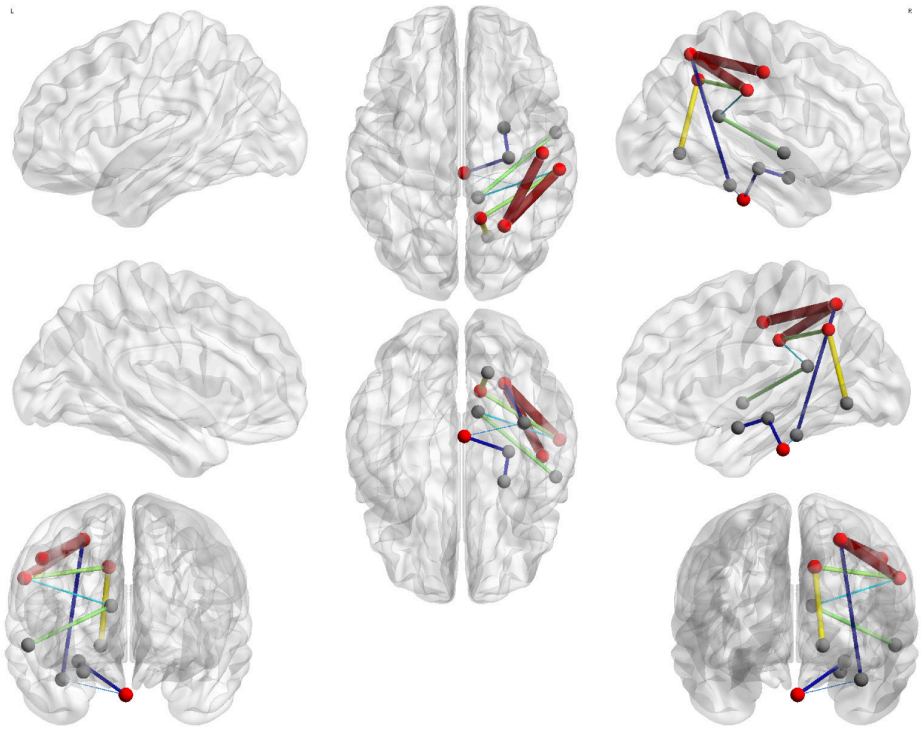

(b)

Figure 4.4: Difference of *connection probability means* for patients and controls

Table 4.3: Global network measures of the entire network

Network measure	**Healthy controls** Mean ± SD	**ALS patients** Mean ± SD	**p**
Efficiency	1.14e-3 ± 3.73e-5	1.14e-3 ± 4.29e-5	0.64
Clustering Coefficient	1.87e-4 ± 3.66e-5	1.82e-4 ± 3.82e-5	0.62
Characteristic Path Length	1.46e3 ± 1.47e2	1.45e3 ± 1.55e2	0.86
Small World*	2.19 ± 1.68	2.02 ± 2.13	0.84

* not normally distributed, Mann-Whitney U test was used instead of a t-test

4.3 Statistics of Network Measures

Beside the NBS Analysis, different network measures were computed for the whole network and the affected subnetwork. The measures of healthy controls and ALS patients where compared with a t- or a Mann-Whitney-U test.

4.3.1 Analysis of the entire Network

4.3.1.1 Global Network Measures: Efficiency, Clustering Coefficient, char. Path Length and Small World Coefficient

Global network measures of the entire network showed no significant differences between controls and patients. The results are given in table 4.3

Global network measures of the patients were correlated with the *ALSFRS-R*, the duration (in months) and the progression. Significant results where found when correlating the duration with the efficiency ($r = 0.49, p = 0.046$) - showing a higher efficiency in patients with a longer disease duration (see figure: 4.5).

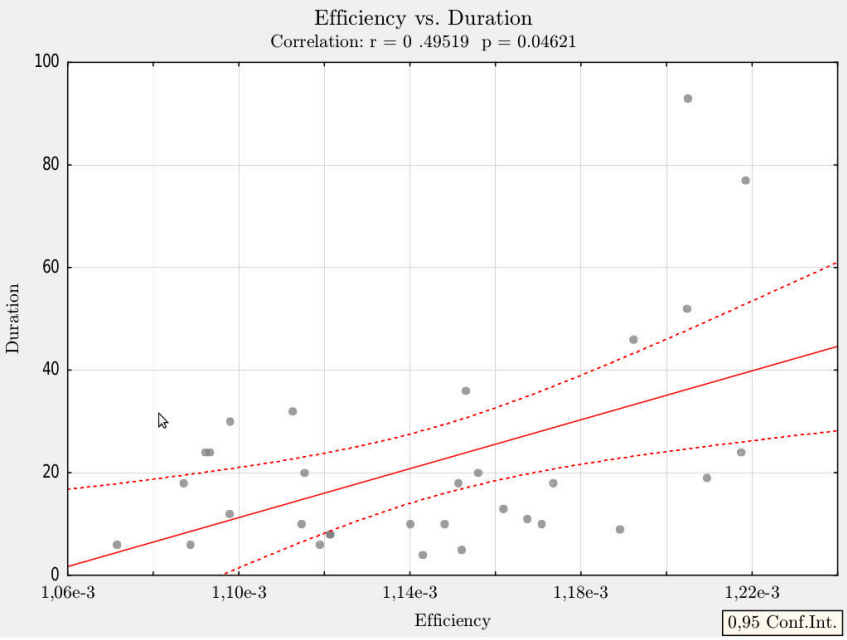

Figure 4.5: positive correlation of efficiency and disease duration. The red dashed line markes the 95% confidence intervall

4.3.2 Analysis of the affected subnetwork

The affected subnetwork was extracted and has undergone the same analysis as the entire network before.

4.3.2.1 Global Network Measures: Efficiency, Clustering Coefficient, char. Path Length, Small World Coefficient and Strength

No significant differences where found when looking at the global network measures of the affected subnetwork, but a borderline significance ($p = 0.06$) for the *clustering coefficient* was observed. This network measure is *higher* in patients, therefore showing a higher segregation of the affected subnetwork. The result is shown in table 4.4

Table 4.4: global network measures of affected subnetwork

Global network measure	**Healthy controls** Mean ± SD	**ALS patients** Mean ± SD	***p***
Efficiency	1.82e43 ± 1.80e-4	1.89e-3 ± 1.83e-4	0.14
Clustering Coefficient	4.53e-4 ± 9.06e-5	4.93e-4 ± 7.97e-5	0.06
Characteristic Path Length	9.77e2 ± 1.39e2	1.06e3 ± 2.79e2	0.12
Small World	1.01 ± 5.08e-2	1.00 ± 6.81e-2	0.63
Strength	0.13 ± 1.25e-2	0.13 ± 1.33e-2	0.22

4.3.2.2 Local Network Measures: Local Efficiency, Local Clustering Coefficient, Local Strength

The local network measures of all affected nodes of the subnetwork are listed in table 4.5.

Table 4.5: local network measures of affected subnetwork

		Healthy controls	**ALS patients**	***p***
Node	Local network measure	Mean ± SD	Mean ± SD	
right isthmus of cingulate gyrus	Efficiency (x10^{-4})	5.68 ± 1.80	6.05 ± 1.87	0.42
	Clustering Coefficient (x10^{-4})	4.71 ± 1.59	4.80 ± 1.52	0.81
	Strength (x10^{-2})	1.15 ± 0.28	1.10 ± 0.20	0.48
right postcentral gyrus	Efficiency (x10^{-4})	8.09 ± 2.67	8.46 ± 2.39	0.55
	Clustering Coefficient (x10^{-4})	6.07 ± 2.18	6.71 ± 1.90	0.21
	Strength (x10^{-2})	1.21 ± 0.18	1.26 ± 0.23	0.28
right supramarginal gyrus	Efficiency (x10^{-4}) *	6.57 ± 3.19	10.52 ± 5.49	0.000116
	Clustering Coefficient (x10^{-4}) *	4.89 ± 2.41	7.59 ± 2.04	0.00242
	Strength (x10^{-2})	1.37 ± 0.19	1.45 ± 0.31	0.0058
right superior parietal cortex	Efficiency (x10^{-4})	9.05 ± 1.84	9.00 ± 2.16	0.92
	Clustering Coefficient (x10^{-4})	5.89 ± 1.28	6.10 ± 1.26	0.51
	Strength (x10^{-2})	2.17 ± 0.29	2.31 ± 0.32	0.03
right precuneus	Efficiency (x10^{-4})	8.47 ± 2.07	9.17 ± 1.51	0.13
	Clustering Coefficient (x10^{-4})	5.86 ± 1.45	6.29 ± 1.13	0.20
	Strength (x10^{-2}) *	2.50 ± 0.38	2.59 ± 0.36	0.58
right lingual gyrus	Efficiency (x10^{-4})	8.03 ± 2.60	8.24 ± 2.49	0.73
	Clustering Coefficient (x10^{-4})	6.02 ± 2.16	6.15 ± 2.03	0.81
	Strength (x10^{-3})	8.60 ± 0.22	8.81 ± 0.23	0.72
right fusiform gyrus	Efficiency (x10^{-4})	4.83 ± 1.79	5.56 ± 2.26	0.15
	Clustering Coefficient (x10^{-4})	3.80 ± 1.55	4.34 ± 1.83	0.21
	Strength (x10^{-2})	8.25 ± 0.17	8.14 ± 0.26	0.84
right superior temporal gyrus	Efficiency (x10^{-4})	6.69 ± 2.70	7.18 ± 2.14	0.43
	Clustering Coefficient (x10^{-4})	4.01 ± 1.64	4.20 ± 1.41	0.46
	Strength (x10^{-3})	8.45 ± 0.25	9.36 ± 0.32	0.21
right hippocampus	Efficiency (x10^{-4})	8.63 ± 1.74	8.03 ± 2.37	0.24
	Clustering Coefficient (x10^{-4})	4.95 ± 1.03	4.56 ± 1.48	0.22
	Strength (x10^{-3})	1.14 ± 0.23	1.03 ± 0.30	0.13
right amygdala	Efficiency (x10^{-4})	1.98 ± 0.76	1.88 ± 0.69	0.59
	Clustering Coefficient (x10^{-4})	1.48 ± 0.57	1.36 ± 0.49	0.38
	Strength (x10^{-3})	0.29 ± 0.06	0.27 ± 0.07	0.15
Brainstem	Efficiency (x10^{-4})	3.01 ± 1.09	3.02 ± 1.22	0.95
	Clustering Coefficient (x10^{-4})	2.09 ± 0.80	2.07 ± 0.90	0.89
	Strength (x10^{-3})	0.27 ± 0.07	0.23 ± 0.09	0.08

* not normally distributed, Mann-Whitney U test was used instead of a *t*-test

The *right supramarginal gyrus* showed significantly higher local efficiency, local clustering coefficient and local strength. Another difference was found in the *right superior parietal cortex* as it shows a higher local strength in ALS patients compared to healthy controls. The brainstem, as well as other core parts of the brain, had lower local strengths in ALS-patients. However, these measures did not reach significance level.

Positive correlation of global clustering coefficient and global strength of the affected subnetwork The global network measures of the affected subnetwork did not show any significant changes, although a borderline significance for a higher clustering coefficient in ALS patient was observed. Therefore this network measure was investigated further. A positive correlation of the clustering coefficient and the progression was found ($p = 0.04, r = 0.40$, figure 4.6). Another global network measure, the strength, also correlated with the disease progression, showing a higher strength of the affected subnetwork in ALS patients (see figure 4.7, $p = 0.17, r = 0.40$). Both clustering and strength of the network increase with the progression of the disease.

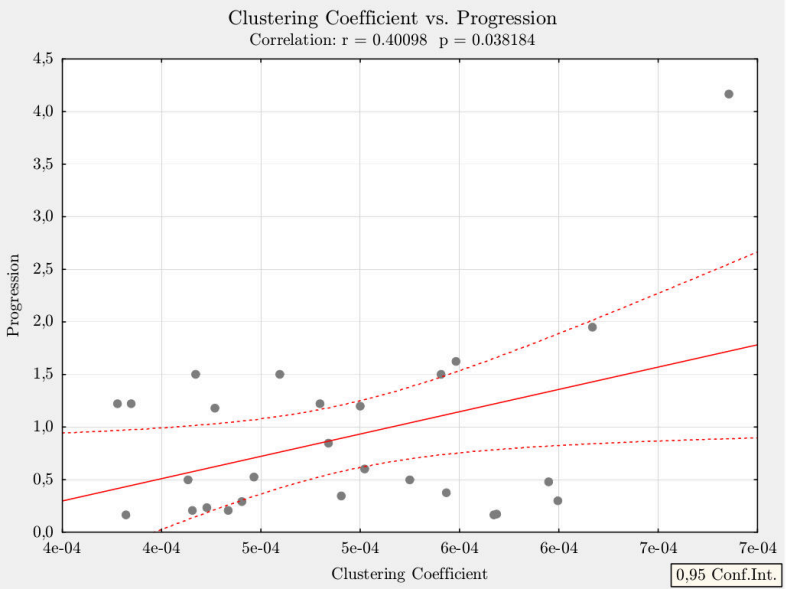

Figure 4.6: positive correlation of clustering coefficient of the affected subnetwork and the progression, the red dashed line markes the 95% confidence interval

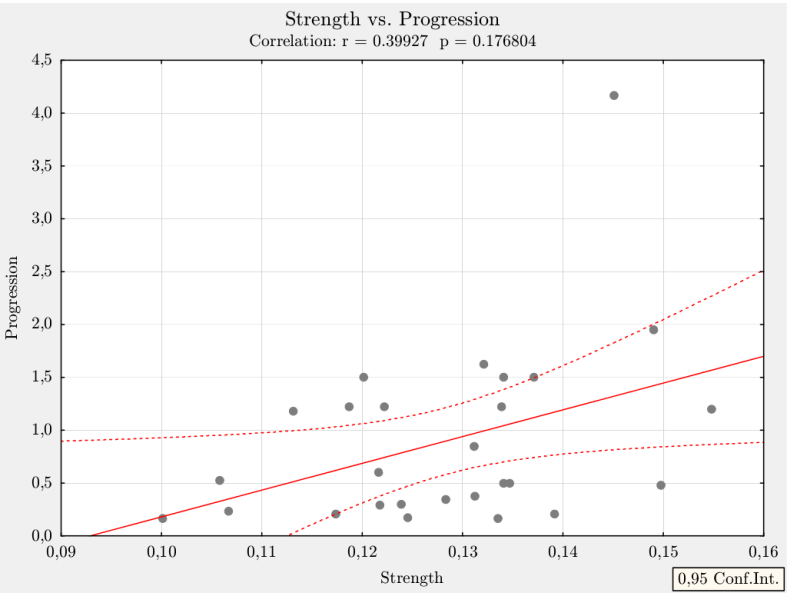

Figure 4.7: positive correlation of strength of the affected subnetwork and the progression, the red dashed line marks the 95% confidence interval

5 Discussion and Conclusion

The aim of this thesis was to explore the sensitivity of structual connectivity in patients with ALS. It was found that structural connectivity is changed in ALS patients compared to healthy controls. This difference is projected to a small subnetwork of the entire brain network.

A F-test was used as statistical test in Network-based statistics. Hence any differences were investigated with a test of *variance-homogenity*. The identified subnetwork showed higher variances of the connection probabilities in this area.

When using a t-test, which compares the means of two samples of a distribution, it was not possible to identify an impaired subnetwork. This is also compatible with the results of other studies of ALS brain-networks ([15],[71]). In contrast to this thesis, Buchanan et. al. and Verstraete et. al. then used a different type of connectivity measure as they generated FA-weighted maps of connectivity. It is well known that the fractional anisotropy is lower in ALS patients ([72],[17],[51],[2],[3]) hence it is not unexpected that a network of FA-weighted connections lower in patients was found - As the FA-connectivity measure was *lower* in ALS patients the identified subnetwork was defined as „impaired“.

In this thesis it was shown that the *variance of the connectivity probabilities* of ALS patients is *higher* in a defined are and therfore one cannot speak of a „disconnected“ or „impaired“ subnetwork.

Further investigation focussed on this subnetwork. The differences in connectivity might be found exactly there. As it is known from other studies ([15],[71]), studying the connectome and its network measures *as a whole* does not show any significant differences in ALS

patients. This finding is in line to our calculation of global network measures of the entire network (see table 4.3 for the listing of the global network measures of the entire network).

The location of the affected subnetwork Interesting is the fact, that this small subnetwork is part of the corticospinal-tract which plays a crucial role in motor development and movement. Five of eleven affected nodes (regions) are part of this major fiber tract of the human brain. (The CST nodes are marked in red in figure 4.4.) A few regions which are part of the CST (e.g. the *internal capsule*) where not parcellated as a seperate region in the segmentation process, but however, it was possible to assign the major regions of CST origin (primary motor cortex, supplementary motor cortex, somatosensory cortex) and the brain stem to the parcellated brain regions. It is known that ALS is a disease which affects both upper and lower motor neurons, but the exact way of degeneration is not fully discovered yet. Another study [71] also identified an impaired subnetwork, which is part of the main motor regions of the brain.
All of the affected regions (except the brain stem) are part of the *right* hemisphere. A recent study [72] also revealed changes in Mean Diffusivity and Magnetization Transfer in the right corticospinaltract whereas the left one did not show significant differences. Other studies, however, found changes in the left corticospinal tract.

Comparing the means of connectivity probability When comparing the *means* of the connection probabilities of the patients and controls it was found that the superior connections (right superior parietal cortex - right postcentral cortex; right superior parietal cortex - right supramarginal gyrus; right supramarginal gyrus - right isthmus of cingulate cortex; right supramarginal gyrus - right precuneus cortex) are higher in ALS patients than in healthy controls, but lower in the inferior connections (right superior parietal cortex - right fusiform gyrus; right hippocampus - right amygdala; right fusiform gyrus - brain stem; right hippocampus - brain stem) as it is shown in table 4.2. This finding is not what one may expect, but it fits to results of other studies, which showed a higher

mean diffusivity in ALS patients ([2],[3],[51]). On the contrary the connectivity in the core parts of the brain is reduced. The superior connections might compensate the lower connectivity in the core parts of the brain to a certain extent.
To inspect the affected network further topological network measures were calculated for both the entire network as well as the affected subnetwork.

Global network measures of the affected subnetwork As shown in table 4.4, global network measures of the affected subnetwork did not show any significant differences, although the clustering coefficient nearly reached significance level, showing a *higher* clustering coefficient in ALS patients.
These network measures were correlated with three important markers of disease progression: The ALSFRS-R, the duration of the disease and the progression (calculated as shown in [51]).
The clustering coefficient, as well as the strength of the affected subnetwork correlated with disease progression. Both measures increase with a stronger disease progression.
Correlation between DTI-derived measures and disease progression were already found earlier: Filippini et al. ([25]) and Iwata et al. ([44]) discovered a positive correlation of disease progression and Fractional Anisotropy in ALS patients, other groups ([3],[17]) found a negative correlation of Fractional Anisotropy within the Corticospinal tract and disease progression.
The clustering coefficient is a measure of the fraction of weighted triangles around a node; it is higher if the weights around the node are higher or the number of triangles around a node is higher (see figure 5.1).

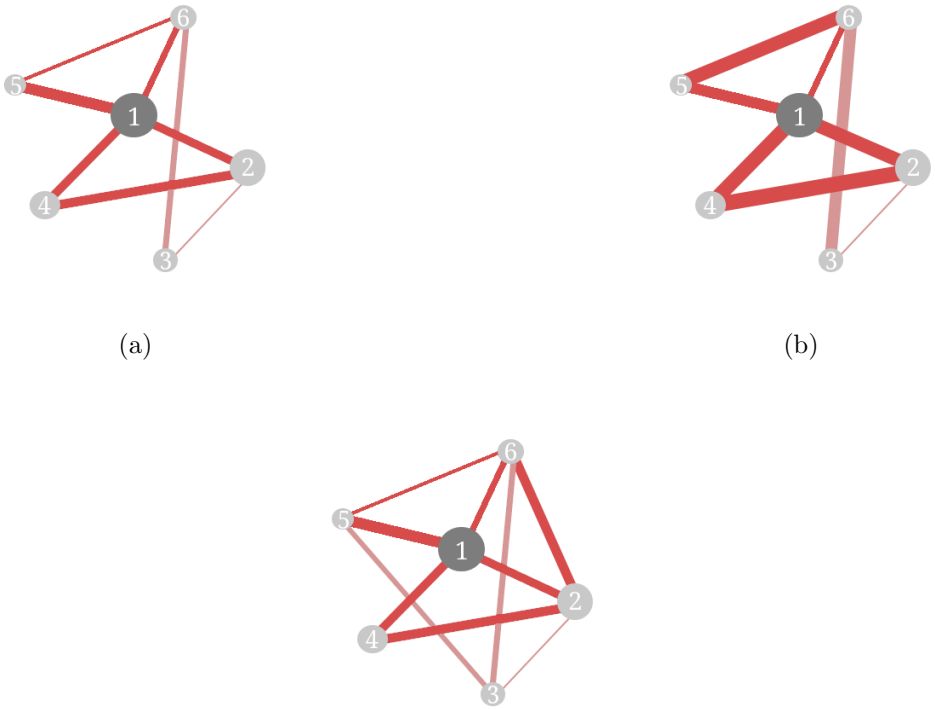

Figure 5.1: Higher clustering coefficient and strength of node 1 in (b) and (c) compared to (a). In (b) the higher clustering coefficient derives from higher weights around the node; in (c) the fraction of triangles is higher (Triangles of node 1 are drawn darker)

The higher clustering coefficient thus can have two reasons - more or stronger connections in the affected subnetwork. The reason of the higher diffusivity in ALS patients is not yet found, but it may be related with an increased proliferation of glial cells and the extracellular matrix expansion [17],[72]. Contrary to our finding of an increased connectivity in patients with stronger progression Ciccarelli et al. [17] found a decreased connectivity. In contrast they had done a comparision of the distribution of the voxel connectivity measures in the CST. The CST was extracted above the internal capsule and the connectivity to the motor regions of the cortex for every voxel in the CST was calculated. The

distributions of the connectivity measures were compared groupwise whereas they only took the tail of the distribution (showing the high connectivity measures which are found in the core of the CST). This method is in total different to the one used here. Another remarkable difference to our result was that the changes they found were located in the *left* CST.
The strength is calculated as sum of all network weights. No significant differences where found with a group-wise comparision but this measure also correlated positively with disease progression.

Local network measures of the affected subnetwork The local network measures showed a higher clustering coefficient, strength and efficiency in the right supramarginal gyrus. All these measures implicate that this node is better embedded in the network structure in ALS. This finding fits to the higher connectivity in the superior part of the affected brain network.
The superior parietal cortex also showed a higher *local strength* in patients which is caused by a higher connection probability to the neighbour nodes.
Local network measures of the inferior part of the subnetwork are in general lower in patients, however, significance level was not reached here.

All of these effects can be described by higher connectivity measures in the coronal regions of the brain and lower values in the brain-stem parts. These connectivity measures also correlated with disease progression, showing higher connectivity measures in patients with a faster progressing disease. The reason why connectivity is increased, cannot be determined from this data and further research has to be done. As it was shown in other studies [71],[72]) fiber tracts are still present in ALS but they may have undergone some alteration of microstructural organization. This alteration can manifest in an decreased fractional anisotropy ([2],[51],[17],[72],[15],[71]), in an increased Mean Diffusivity ([51],[2],

[3]) or an increased radial diffusivity ([3],[72]). It is still not clear how these measures interact exactely and what reason on microstructural changes is underlying.
Another study found an increase in the magnetization transfer ratio ([72]) in the right CST. They assumed that the higher MTR is caused by an accumulation of pathological protein aggregates and therfore showing a higher macromolecular fraction.

Remarks on the used methods Connectivity measures were investigated with an probabilistic approach. [11] This approach and its extension [12] are widely used because it can resolve multiple fibers per voxel and therefore solve the problem of crossing or kissing fibers. Nevertheless we used a model with only one fibre per voxel, as it was shown that crossing fibers are resolvable only with a high number of independent diffusion gradient directions or higher b-values (see figure 5.2).

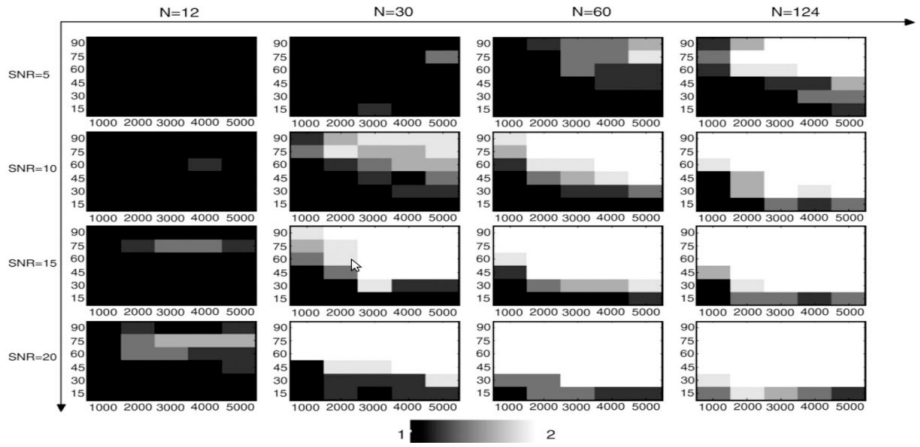

Figure 5.2: Study of Behrens et al. [12]: They generated a voxel with two crossing fibers and tried to find them with differnt gradient directions N (main x-axis) and SNRs (main $y-axis$), as well as with different b-values and seperation angles of the two fibers (main x- and y-axis respectively); with a low b-value of 1000 mm/s^2 it is impossible to find the crossing two fibers, only one fiber is found per voxel; image taken from [12]

Differences in brain connectivity were explored with the method of Zalesky [78]. The high number of possible connections (with 83 regions more than three thousand connections are possible) makes statistical testing prone to misinterpretations. When making such a high number of statistical tests a significant change can be found just by chance. This problem is called *multiple testing problem* and several correction procedures exist. Here, we used permutation testing to find the distribution of the maximal component size and marked an identified subnetwork as significant if the component size was only higher in 5% of the permutations. This method was widely used in many other studies ([15],[71],[34]) to find any differences in neurodegenerative and inflammatory diseases.
Weighted network measures were used to cope with the problem of thresholding. All of the calculations were done on raw connectivity matrices and no thresholding or edge discarding was done to control false positives (as it was done for example in [15] or [71]). All of these binarizing or normalizing procedures are somehow based on arbitrary set thresholds and assumptions. Additionally, Rodrigues et al. [57] showed that connectome variability is even higher after binarizing.

Conclusion Structural connectivity in ALS patients by using a network-based approach revealed further inside look into disease's location. Additionally, severity of disease correlated with network measures derived from a subnetwork of the entire brain.
Connectivity in ALS is partly stronger and the network is better connected in disease, which is somehow unexpected. However, many different parameters contribute to a better connectivity measure and it was already shown in other studies ([51],[2], [3]) that the mean diffusivity is higher in regions of ALS-diseased brains. Increased diffusivity might contribute to fiber-tracts which connect two regions, yet leading to higher connectivity measure.
Structural connectivity was investigated with a network-based approach. However, the basis of the derived measures is diffusion MRI and its parameters. All of the DTI-derived parameter contribute to the calculated connectivity measure. The problem of interpreting such a „disconnected“, „stronger“ or „affected“ network is, that it is still not known

how microstructural changes exactly affect measures like Fractional Anisotropy or Mean Diffusivity and hence the connectivity.
The disease of ALS is related to a proliferation of glial cells, extracellular matrix expansion and intraneuron abnormalities. [42] The connection to diffusion MRI is that myelin breakdown is associated with increased perpendicular diffusivity and decreased Fractional Anisotropy. [9]
„To understand the functioning of a network, one must know its elements and their interconnections“ [67] stated Sporns in 2005. The interconnections in diffusion MRI and structural connectomics are still prone to misinterpretations. Therefore it remains challenging to make an explicit statement of how ALS affects the brain-network.

To conclude, this work demonstrated that structural connectivity gives complementary information about pathological processes in ALS and revealed *clustering coefficient* and *strength* of the affected subnetwork as an additional marker of disease progression rate.

Index of Abbreviations

ALS Amyotrophic Lateral Sclerosis

ALSFRS-R Amyotrophic Lateral Sclerosis Functional Rating Scale-Revised

CST Cortico Spinal Tract

DTI Diffusion Tensor Imaging

FA Fractional Anisotropy

GM Grey Matter

MD Mean Diffusivity

MRI Magnetic Resonance Imaging/Image

SMA Supplementary Motor Areal

SD Standard Derivation

TBSS Tract Based Spatial Statistics

VBM Voxel Based Morphometry

WM White Matter

Appendix

Table 5.1: Listing of ROIs

#	color	hemisphere	Region	Label	*freesurfer* name
1		Right	Lateral orbital frontal cortex	rh.lateralorbitofrontal	ctx-rh-lateralorbitofrontal
2		Right	Pars orbitalis	rh.parsorbitalis	ctx-rh-parsorbitalis
3		Right	Frontal pole	rh.frontalpole	ctx-rh-frontalpole
4		Right	Medial orbital frontal cortex	rh.medialorbitofrontal	ctx-rh-medialorbitofrontal
5		Right	Pars triangularis	rh.parstriangularis	ctx-rh-parstriangularis
6		Right	Pars opercularis	rh.parsopercularis	ctx-rh-parsopercularis
7		Right	Rostral middle frontal gyrus	rh.rostralmiddlefrontal	ctx-rh-rostralmiddlefrontal
8		Right	Superior frontal gyrus	rh.superiorfrontal	ctx-rh-superiorfrontal
9		Right	Caudal middle frontal gyrus	rh.caudalmiddlefrontal	ctx-rh-caudalmiddlefrontal
10		Right	Precentral gyrus	rh.precentral	ctx-rh-precentral
11		Right	Paracentral lobule	rh.paracentral	ctx-rh-paracentral
12		Right	Rostral anterior cingulate cortex	rh.rostralanteriorcingulate	ctx-rh-rostralanteriorcingulate
13		Right	Caudal anterior-cingulate cortex	rh.caudalanteriorcingulate	ctx-rh-caudalanteriorcingulate
14		Right	Posterior-cingulate cortex	rh.posteriorcingulate	ctx-rh-posteriorcingulate
15		Right	Isthmus – cingulate cortex	rh.isthmuscingulate	ctx-rh-isthmuscingulate
16		Right	Postcentral gyrus	rh.postcentral	ctx-rh-postcentral
17		Right	Supramarginal gyrus	rh.supramarginal	ctx-rh-supramarginal
18		Right	Superior parietal cortex	rh.superiorparietal	ctx-rh-superiorparietal
19		Right	Inferior parietal cortex	rh.inferiorparietal	ctx-rh-inferiorparietal
20		Right	Precuneus cortex	rh.precuneus	ctx-rh-precuneus
21		Right	Cuneus cortex	rh.cuneus	ctx-rh-cuneus
22		Right	Pericalcarine cortex	rh.pericalcarine	ctx-rh-pericalcarine
23		Right	Lateral occipital cortex	rh.lateraloccipital	ctx-rh-lateraloccipital
24		Right	Lingual gyrus	rh.lingual	ctx-rh-lingual
25		Right	Fusiform gyrus	rh.fusiform	ctx-rh-fusiform
26		Right	Parahippocampal gyrus	rh.parahippocampal	ctx-rh-parahippocampal
27		Right	Entorhinal cortex	rh.entorhinal	ctx-rh-entorhinal
28		Right	Temporal pole	rh.temporalpole	ctx-rh-temporalpole
29		Right	Inferior temporal gyrus	rh.inferiortemporal	ctx-rh-inferiortemporal

Table 5.1: Listing of ROIs

#	color	hemisphere	Region	Label	*freesurfer* name
30		Right	Middle temporal gyrus	rh.middletemporal	ctx-rh-middletemporal
31		Right	Banks superior temporal sulcus	rh.bankssts	ctx-rh-bankssts
32		Right	Superior temporal gyrus	rh.superiortemporal	ctx-rh-superiortemporal
33		Right	Transverse temporal cortex	rh.transversetemporal	ctx-rh-transversetemporal
34		Right	Insula	rh.insula	ctx-rh-insula
35		Right	Thalamus	Right-Thalamus-Proper	Right-Thalamus-Proper
36		Right	Caudate	Right-Caudate	Right-Caudate
37		Right	Putamen	Right-Putamen	Right-Putamen
38		Right	Pallidum	Right-Pallidum	Right-Pallidum
39		Right	Accumbens area	Right-Accumbens-area	Right-Accumbens-area
40		Right	Hippocampus	Right-Hippocampus	Right-Hippocampus
41		Right	Amygdala	Right-Amygdala	Right-Amygdala
42		Left	Lateral orbital frontal cortex	lh.lateralorbitofrontal	ctx-lh-lateralorbitofrontal
43		Left	Pars orbitalis	lh.parsorbitalis	ctx-lh-parsorbitalis
44		Left	Frontal pole	lh.frontalpole	ctx-lh-frontalpole
45		Left	Medial orbital frontal cortex	lh.medialorbitofrontal	ctx-lh-medialorbitofrontal
46		Left	Pars triangularis	lh.parstriangularis	ctx-lh-parstriangularis
47		Left	Pars opercularis	lh.parsopercularis	ctx-lh-parsopercularis
48		Left	Rostral middle frontal gyrus	lh.rostralmiddlefrontal	ctx-lh-rostralmiddlefrontal
49		Left	Superior frontal gyrus	lh.superiorfrontal	ctx-lh-superiorfrontal
50		Left	Caudal middle frontal gyrus	lh.caudalmiddlefrontal	ctx-lh-caudalmiddlefrontal
51		Left	Precentral gyrus	lh.precentral	ctx-lh-precentral
52		Left	Paracentral lobule	lh.paracentral	ctx-lh-paracentral
53		Left	Rostral anterior cingulate cortex	lh.rostralanteriorcingulate	ctx-lh-rostralanteriorcingulate
54		Left	Caudal anterior-cingulate cortex	lh.caudalanteriorcingulate	ctx-lh-caudalanteriorcingulate
55		Left	Posterior-cingulate cortex	lh.posteriorcingulate	ctx-lh-posteriorcingulate
56		Left	Isthmus – cingulate cortex	lh.isthmuscingulate	ctx-lh-isthmuscingulate
57		Left	Postcentral gyrus	lh.postcentral	ctx-lh-postcentral
58		Left	Supramarginal gyrus	lh.supramarginal	ctx-lh-supramarginal
59		Left	Superior parietal cortex	lh.superiorparietal	ctx-lh-superiorparietal
60		Left	Inferior parietal cortex	lh.inferiorparietal	ctx-lh-inferiorparietal
61		Left	Precuneus cortex	lh.precuneus	ctx-lh-precuneus
62		Left	Cuneus cortex	lh.cuneus	ctx-lh-cuneus
63		Left	Pericalcarine cortex	lh.pericalcarine	ctx-lh-pericalcarine
64		Left	Lateral occipital cortex	lh.lateraloccipital	ctx-lh-lateraloccipital
65		Left	Lingual gyrus	lh.lingual	ctx-lh-lingual
66		Left	Fusiform gyrus	lh.fusiform	ctx-lh-fusiform
67		Left	Parahippocampal gyrus	lh.parahippocampal	ctx-lh-parahippocampal
68		Left	Entorhinal cortex	lh.entorhinal	ctx-lh-entorhinal
69		Left	Temporal pole	lh.temporalpole	ctx-lh-temporalpole
70		Left	Inferior temporal gyrus	lh.inferiortemporal	ctx-lh-inferiortemporal

Table 5.1: Listing of ROIs

#	color	hemisphere	Region	Label	*freesurfer* name
71		Left	Middle temporal gyrus	lh.middletemporal	ctx-lh-middletemporal
72		Left	Banks superior temporal sulcus	lh.bankssts	ctx-lh-bankssts
73		Left	Superior temporal gyrus	lh.superiortemporal	ctx-lh-superiortemporal
74		Left	Transverse temporal cortex	lh.transversetemporal	ctx-lh-transversetemporal
75		Left	Insula	lh.insula	ctx-lh-insula
76		Left	Thalamus	Left-Thalamus-Proper	Left-Thalamus-Proper
77		Left	Caudate	Left-Caudate	Left-Caudate
78		Left	Putamen	Left-Putamen	Left-Putamen
79		Left	Pallidum	Left-Pallidum	Left-Pallidum
80		Left	Accumbens area	Left-Accumbens-area	Left-Accumbens-area
81		Left	Hippocampus	Left-Hippocampus	Left-Hippocampus
82		Left	Amygdala	Left-Amygdala	Left-Amygdala
83		-	Brain Stem	Brain-Stem	Brain-Stem

Bibliography

[1] Kumar Abhinav, Fang-Chang Yeh, Sudhir Pathak, Robert M. Friedlander, and Juan C. Fernandez-Miranda. Advanced diffusion MRI fiber tracking in neurosurgical and neurodegenerative disorders and neuroanatomical studies: A review. *Biochimica et Biophysica Acta (BBA) - Molecular Basis of Disease*, 1842(11):2286–2297, 2014. ISSN 09254439. doi: 10.1016/j.bbadis.2014.08.002. URL `http://www.sciencedirect.com/science/article/pii/S0925443914002555`.

[2] F. Agosta, E. Pagani, M. a. Rocca, D. Caputo, M. Perini, F. Salvi, a. Prelle, and Massimo Filippi. Voxel-based morphometry study of brain volumetry and diffusivity in amyotrophic lateral sclerosis patients with mild disability. *Human Brain Mapping*, 28(March):1430–1438, 2007. ISSN 10659471. doi: 10.1002/hbm.20364.

[3] F. Agosta, E. Pagani, M. Petrolini, D. Caputo, M. Perini, a. Prelle, F. Salvi, and Massimo Filippi. Assessment of white matter tract damage in patients with amyotrophic lateral sclerosis: A diffusion tensor MR imaging tractography study. *American Journal of Neuroradiology*, 31(March 2006):1457–1461, 2010. ISSN 01956108. doi: 10.3174/ajnr.A2105.

[4] J Ashburner and K J Friston. Voxel-based morphometry–the methods. *NeuroImage*, 11:805–821, 2000. ISSN 1053-8119. doi: 10.1006/nimg.2000.0582.

[5] Kim Barrett, Heddwen Brooks, Scott Boitano, and Susan Barman. *Ganong's review*

of medical physiology. 2010. ISBN 9780071605687.

[6] P J Basser, J Mattiello, and D LeBihan. MR diffusion tensor spectroscopy and imaging. *Biophysical journal*, 66(1):259–267, 1994. ISSN 0006-3495. doi: 10.1016/S0006-3495(94)80775-1. URL `http://dx.doi.org/10.1016/S0006-3495(94)80775-1`.

[7] Peter J Basser and Derek K Jones. Diffusion-tensor MRI: theory, experimental design and data analysis - a technical review. *NMR in biomedicine*, 15(7-8):456–67, 2002. ISSN 0952-3480. doi: 10.1002/nbm.783. URL `http://www.ncbi.nlm.nih.gov/pubmed/12489095`.

[8] Bassett Danielle S; Bullmore Edward. Human Brain Networks in Health and Disease. *Curr. Opin. Neurology*, 22(4):340–347, 2009. doi: 10.1097/WCO.0b013e32832d93dd. Human.

[9] Christian Beaulieu. The basis of anisotropic water diffusion in the nervous system - A technical review. *NMR in Biomedicine*, 15(7-8):435–455, 2002. ISSN 09523480. doi: 10.1002/nbm.782.

[10] Peter Bede and Orla Hardiman. Lessons of ALS imaging: Pitfalls and future directions - A critical review. *NeuroImage. Clinical*, 4:436–443, January 2014. ISSN 2213-1582. doi: 10.1016/j.nicl.2014.02.011. URL `http://www.pubmedcentral.nih.gov/articlerender.fcgi?artid=3950559&tool=pmcentrez&rendertype=abstract`.

[11] T E J Behrens, M W Woolrich, M Jenkinson, H Johansen-Berg, R G Nunes, S Clare, P M Matthews, J M Brady, and S M Smith. Characterization and propagation of uncertainty in diffusion-weighted MR imaging. *Magnetic resonance in medicine : official journal of the Society of Magnetic Resonance in Medicine / Society of Magnetic Resonance in Medicine*, 50(5):1077–88, November 2003. ISSN 0740-3194. doi: 10.1002/mrm.10609. URL `http://www.ncbi.nlm.nih.gov/pubmed/14587019`.

[12] T E J Behrens, H Johansen Berg, S Jbabdi, M F S Rushworth, and M W Woolrich. Probabilistic diffusion tractography with multiple fibre orientations: What can we gain? *NeuroImage*, 34(1):144–55, January 2007. ISSN 1053-8119. doi: 10.1016/j.neuroimage.2006.09.018. URL `http://www.ncbi.nlm.nih.gov/pubmed/17070705`.

[13] B R Brooks, R G Miller, M Swash, and T L Munsat. El Escorial revisited: revised criteria for the diagnosis of amyotrophic lateral sclerosis. *Amyotrophic lateral sclerosis and other motor neuron disorders : official publication of the World Federation of Neurology, Research Group on Motor Neuron Diseases*, 1(5):293–299, December 2000. ISSN 1466-0822 (Print).

[14] BR Brooks. El Escorial World Federation of Neurology criteria for the diagnosis of amyotrophic lateral sclerosis. Subcommittee on Motor Neuron Diseases/Amyotrophic Lateral Sclerosis of the World Federation of Neurology Research Group on Neuromuscular Diseases and th. *J Neurol Sci.*, 124(96-107), 1994.

[15] Colin R. Buchanan, Lewis D. Pettit, Amos J. Storkey, Sharon Abrahams, and Mark E. Bastin. Reduced structural connectivity within a prefrontal-motor-subcortical network in amyotrophic lateral sclerosis. *Journal of Magnetic Resonance Imaging*, 00, 2014. ISSN 10531807. doi: 10.1002/jmri.24695.

[16] Edward T Bullmore and Danielle S Bassett. Brain graphs: graphical models of the human brain connectome. *Annual review of clinical psychology*, 7:113–40, January 2011. ISSN 1548-5951. doi: 10.1146/annurev-clinpsy-040510-143934. URL `http://www.ncbi.nlm.nih.gov/pubmed/21128784`.

[17] O. Ciccarelli, T. E. Behrens, D. R. Altmann, R. W. Orrell, R. S. Howard, H. Johansen-Berg, D. H. Miller, P. M. Matthews, and a. J. Thompson. Probabilistic diffusion tractography: A potential tool to assess the rate of disease progression in amyotrophic lateral sclerosis. *Brain*, 129:1859–1871, 2006. ISSN 00068950. doi: 10.1093/brain/awl100.

[18] M. Cirillo, F. Esposito, Gioacchino Tedeschi, G. Caiazzo, a. Sagnelli, G. Piccirillo, R. Conforti, F. Tortora, M. R. Monsurrò, S. Cirillo, and F. Trojsi. Widespread microstructural white matter involvement in amyotrophic lateral sclerosis: A whole-brain DTI study. *American Journal of Neuroradiology*, 33:1102–1108, 2012. ISSN 01956108. doi: 10.3174/ajnr.A2918.

[19] Mirco Cosottini, Marco Giannelli, Gabriele Siciliano, Guido Lazzarotti, Maria Chiara Michelassi, Alberto Del Corona, Carlo Bartolozzi, and Luigi Murri. Diffusion-tensor MR imaging of corticospinal tract in amyotrophic lateral sclerosis and progressive muscular atrophy. *Radiology*, 237(1):258–264, 2005. ISSN 0033-8419. doi: 10.1148/radiol.2371041506.

[20] Mirco Cosottini, Ilaria Pesaresi, Selina Piazza, Stefano Diciotti, Paolo Cecchi, Serena Fabbri, Cecilia Carlesi, Mario Mascalchi, and Gabriele Siciliano. Structural and functional evaluation of cortical motor areas in Amyotrophic Lateral Sclerosis. *Experimental Neurology*, 234(1):169–180, 2012. ISSN 00144886. doi: 10.1016/j.expneurol.2011.12.024. URL `http://dx.doi.org/10.1016/j.expneurol.2011.12.024`.

[21] R Cameron Craddock, Saad Jbabdi, Chao-Gan Yan, Joshua T Vogelstein, F Xavier Castellanos, Adriana Di Martino, Clare Kelly, Keith Heberlein, Stan Colcombe, and Michael P Milham. Imaging human connectomes at the macroscale. *Nature methods*, 10(6):524–39, June 2013. ISSN 1548-7105. doi: 10.1038/nmeth.2482. URL `http://www.ncbi.nlm.nih.gov/pubmed/23722212`.

[22] Alessandro Daducci, Stephan Gerhard, Alessandra Griffa, Alia Lemkaddem, Leila Cammoun, Xavier Gigandet, Reto Meuli, Patric Hagmann, and Jean-Philippe Thiran. The connectome mapper: an open-source processing pipeline to map connectomes with MRI. *PloS one*, 7(12):e48121, January 2012. ISSN 1932-6203. doi: 10.1371/journal.pone.0048121. URL `http://dx.plos.org/10.1371/journal.pone.0048121http://www.pubmedcentral.nih.gov/articlerender.fcgi?artid=3525592&tool=pmcentrez&rendertype=abstract`.

[23] Marcel a de Reus and Martijn P van den Heuvel. The parcellation-based connectome: limitations and extensions. *NeuroImage*, 80:397–404, October 2013. ISSN 1095-9572. doi: 10.1016/j.neuroimage.2013.03.053. URL http://www.ncbi.nlm.nih.gov/pubmed/23558097.

[24] Rahul S Desikan, Florent Ségonne, Bruce Fischl, Brian T Quinn, Bradford C Dickerson, Deborah Blacker, Randy L Buckner, Anders M Dale, R Paul Maguire, Bradley T Hyman, Marilyn S Albert, and Ronald J Killiany. An automated labeling system for subdividing the human cerebral cortex on MRI scans into gyral based regions of interest. *NeuroImage*, 31(3):968–80, July 2006. ISSN 1053-8119. doi: 10.1016/j.neuroimage.2006.01.021. URL http://www.sciencedirect.com/science/article/pii/S1053811906000437http://www.ncbi.nlm.nih.gov/pubmed/16530430.

[25] N Filippini, G Douaud, C E Mackay, S Knight, K Talbot, and M R Turner. Corpus callosum involvement is a consistent feature of amyotrophic lateral sclerosis. *Neurology*, 75(18):1645–1652, November 2010. ISSN 0028-3878. doi: 10.1212/WNL.0b013e3181fb84d1. URL http://www.ncbi.nlm.nih.gov/pmc/articles/PMC2974368/.

[26] B. Fischl. Automatically Parcellating the Human Cerebral Cortex. *Cerebral Cortex*, 14(1):11–22, January 2004. ISSN 1460-2199. doi: 10.1093/cercor/bhg087. URL http://www.cercor.oupjournals.org/cgi/doi/10.1093/cercor/bhg087http://cercor.oxfordjournals.org/content/14/1/11.short.

[27] B Fischl, a Liu, and a M Dale. Automated manifold surgery: constructing geometrically accurate and topologically correct models of the human cerebral cortex. *IEEE transactions on medical imaging*, 20(1):70–80, January 2001. ISSN 0278-0062. doi: 10.1109/42.906426. URL http://www.ncbi.nlm.nih.gov/pubmed/11293693.

[28] Bruce Fischl, Martin I Sereno, Anders M Dale, Van Essen, I Segmentation, and

Surface Reconstruction. Cortical Surface-Based Analysis. 207:179–194, 1999.

[29] Bruce Fischl, David H Salat, Evelina Busa, Marilyn Albert, Megan Dieterich, Christian Haselgrove, Andre van der Kouwe, Ron Killiany, David Kennedy, Shuna Klaveness, Albert Montillo, Nikos Makris, Bruce Rosen, and Anders M Dale. Whole brain segmentation: automated labeling of neuroanatomical structures in the human brain. *Neuron*, 33(3):341–55, January 2002. ISSN 0896-6273. URL `http://www.ncbi.nlm.nih.gov/pubmed/11832223`.

[30] Bruce Fischl, David H Salat, André J W van der Kouwe, Nikos Makris, Florent Ségonne, Brian T Quinn, and Anders M Dale. Sequence-independent segmentation of magnetic resonance images. *NeuroImage*, 23 Suppl 1:S69–84, January 2004. ISSN 1053-8119. doi: 10.1016/j.neuroimage.2004.07.016. URL `http://www.ncbi.nlm.nih.gov/pubmed/15501102`.

[31] Freesurfer. recon_all. URL `http://surfer.nmr.mgh.harvard.edu/fswiki/recon-all`.

[32] FSL. FMRIB's Diffusion Toolbox - FDT v2.0. URL `http://fsl.fmrib.ox.ac.uk/fsl/fsl-4.1.9/fdt/fdt_eddy.html`.

[33] Xavier Gigandet, Alessandra Griffa, Tobias Kober, Alessandro Daducci, Guillaume Gilbert, Alan Connelly, Patric Hagmann, Reto Meuli, Jean-Philippe Thiran, and Gunnar Krueger. A connectome-based comparison of diffusion MRI schemes. *PloS one*, 8(9):e75061, January 2013. ISSN 1932-6203. URL `http://www.plosone.org/article/info:doi/10.1371/journal.pone.0075061#pone-0075061-g007`.

[34] Alessandra Griffa, Philipp S Baumann, Jean-Philippe Thiran, and Patric Hagmann. Structural connectomics in brain diseases. *NeuroImage*, 80:515–26, October 2013. ISSN 1095-9572. doi: 10.1016/j.neuroimage.2013.04.056. URL `http://www.ncbi.nlm.nih.gov/pubmed/23623973`.

[35] Arthur C. Guyton and John E. Hall. *Textbook of medical physiology*. 2006. ISBN 0721602401.

[36] P Hagmann, O Sporns, N Madan, L Cammoun, R Pienaar, V J Wedeen, R Meuli, J-P Thiran, and P E Grant. White matter maturation reshapes structural connectivity in the late developing human brain. *Proceedings of the National Academy of Sciences of the United States of America*, 107(44):19067–72, November 2010. ISSN 1091-6490. doi: 10.1073/pnas.1009073107. URL `http://www.pubmedcentral.nih.gov/articlerender.fcgi?artid=2973853&tool=pmcentrez&rendertype=abstract`.

[37] Patric Hagmann. From Diffusion MRI to Brain Connectomics. *Science*, 3230, 2005. doi: 10.5075/epfl-thesis-3230. URL `http://www.mendeley.com/catalog/diffusion-mri-brain-connectomics-4/`.

[38] Patric Hagmann, Maciej Kurant, Xavier Gigandet, Patrick Thiran, Van J Wedeen, Reto Meuli, and Jean-Philippe Thiran. Mapping human whole-brain structural networks with diffusion MRI. *PloS one*, 2(7):e597, January 2007. ISSN 1932-6203. URL `http://www.pubmedcentral.nih.gov/articlerender.fcgi?artid=1895920&tool=pmcentrez&rendertype=abstract`.

[39] Patric Hagmann, Leila Cammoun, Xavier Gigandet, Stephan Gerhard, P Ellen Grant, Van Wedeen, Reto Meuli, Jean-Philippe Thiran, Christopher J Honey, and Olaf Sporns. MR connectomics: Principles and challenges. *Journal of neuroscience methods*, 194(1):34–45, December 2010. ISSN 1872-678X. URL `http://www.sciencedirect.com/science/article/pii/S0165027010000361`.

[40] Horst K Hahn and Heinz-otto Peitgen. The Skull Stripping Problem in MRI Solved by a Single 3D Watershed Transform. *Proc. MICCAI*, pages 134–143, 2000.

[41] Tim Hesterberg, David S Ds Moore, Shaun Monaghan, Ashley Clipson, and Rachel Epstein. *Bootstrap Methods and Permutation Tests*, volume 5. 2005. ISBN

2002108463. doi: 10.1002/wics.182. URL `http://seongjoon.com/drupal/files/Bootstrapmethodsandpermutationtests_PBS18.pdf`.

[42] J T Hughes. Pathology of amyotrophic lateral sclerosis. *Advances in neurology*, 36: 61–74, 1982. ISSN 0091-3952 (Print).

[43] Andrei Irimia, Micah C Chambers, Carinna M Torgerson, Maria Filippou, David A Hovda, Jeffry R Alger, Guido Gerig, Arthur W Toga, Paul M Vespa, Ron Kikinis, and John D Van Horn. Patient-tailored connectomics visualization for the assessment of white matter atrophy in traumatic brain injury. *Frontiers in neurology*, 3:10, January 2012. ISSN 1664-2295. doi: 10.3389/fneur.2012.00010. URL `http://www.pubmedcentral.nih.gov/articlerender.fcgi?artid=3275792&tool=pmcentrez&rendertype=abstract`.

[44] Nobue K. Iwata, Justin Y. Kwan, Laura E. Danielian, John a. Butman, Fernanda Tovar-Moll, Elham Bayat, and Mary Kay Floeter. White matter alterations differ in primary lateral sclerosis and amyotrophic lateral sclerosis. *Brain*, 134(9):2642–2655, 2011. ISSN 00068950. doi: 10.1093/brain/awr178.

[45] Brian J Jellison, Aaron S Field, Joshua Medow, Mariana Lazar, M Shariar Salamat, and Andrew L Alexander. Diffusion tensor imaging of cerebral white matter: a pictorial review of physics, fiber tract anatomy, and tumor imaging patterns. *AJNR. American journal of neuroradiology*, 25(3):356–369, March 2004. ISSN 0195-6108 (Print).

[46] M Jenkinson and S Smith. A global optimisation method for robust affine registration of brain images. *Medical image analysis*, 5(2):143–56, June 2001. ISSN 1361-8415. URL `http://www.ncbi.nlm.nih.gov/pubmed/11516708`.

[47] Mark Jenkinson, Peter Bannister, Michael Brady, and Stephen Smith. Improved Optimization for the Robust and Accurate Linear Registration and Motion Correction

of Brain Images. *NeuroImage*, 17(2):825–841, October 2002. ISSN 10538119. doi: 10.1006/nimg.2002.1132. URL http://linkinghub.elsevier.com/retrieve/pii/S1053811902911328.

[48] Ben Jeurissen, Alexander Leemans, Jacques-Donald Tournier, Derek K Jones, and Jan Sijbers. Investigating the prevalence of complex fiber configurations in white matter tissue with diffusion magnetic resonance imaging. *Human brain mapping*, 34(11):2747–66, November 2013. ISSN 1097-0193. doi: 10.1002/hbm.22099. URL http://www.ncbi.nlm.nih.gov/pubmed/22611035.

[49] Michael Kaas, Andrew Witkin, and Demetri Terzopoulos. Snakes: Active Contour Models.pdf. *International Journal of Computer Vision*, 1(4):321–331, 1988.

[50] Marcus Kaiser. A tutorial in connectome analysis: topological and spatial features of brain networks. *NeuroImage*, 57(3):892–907, August 2011. ISSN 1095-9572. URL http://www.sciencedirect.com/science/article/pii/S1053811911005131.

[51] Christian Langkammer, Christian Enzinger, Stefan Quasthoff, Paula Grafenauer, Michaela Soellinger, Franz Fazekas, and Stefan Ropele. Mapping of iron deposition in conjunction with assessment of nerve fiber tract integrity in amyotrophic lateral sclerosis. *Journal of Magnetic Resonance Imaging*, 31:1339–1345, 2010. ISSN 10531807. doi: 10.1002/jmri.22185.

[52] Daniel S Margulies, Joachim Böttger, Aimi Watanabe, and Krzysztof J Gorgolewski. Visualizing the human connectome. *NeuroImage*, 80:445–61, October 2013. ISSN 1095-9572. doi: 10.1016/j.neuroimage.2013.04.111. URL http://www.sciencedirect.com/science/article/pii/S1053811913004709http://www.ncbi.nlm.nih.gov/pubmed/23660027.

[53] OpenDSA. CHAPTER 16 GRAPHS. URL http://algoviz.org/OpenDSA/Books/Everything/html/GraphIntro.html.

[54] Julia P Owen, Yi-Ou Li, Etay Ziv, Zoe Strominger, Jacquelyn Gold, Polina Bukhpun, Mari Wakahiro, Eric J Friedman, Elliott H Sherr, and Pratik Mukherjee. The structural connectome of the human brain in agenesis of the corpus callosum. *NeuroImage*, 70:340–55, April 2013. ISSN 1095-9572. URL `http://www.sciencedirect.com/science/article/pii/S1053811912012165`.

[55] Hanspeter Pfister, Verena Kaynig, Charl P Botha, Stefan Bruckner, and G R Aug. Visualization in Connectomics. *arXiv:1206.1428v2*, pages 1–26, 2012.

[56] Isabella Radl. *Evaluation of Imageprocessing Software BioImage Suite*. PhD thesis, 2012.

[57] Paulo Rodrigues, Alberto Prats-Galino, David Gallardo-Pujol, Pablo Villoslada, Carles Falcon, and Vesna Prckovska. Evaluating structural connectomics in relation to different Q-space sampling techniques. *Medical image computing and computer-assisted intervention : MICCAI ... International Conference on Medical Image Computing and Computer-Assisted Intervention*, 16(Pt 1):671–8, January 2013. URL `http://www.ncbi.nlm.nih.gov/pubmed/24505725`.

[58] Lewis P. Rowland and Neil A. Shneider. Amyotrophic Lateral Sclerosis. *New England Journal of Medicine*, 344(22):1688–1700, 2001.

[59] Mikail Rubinov and Olaf Sporns. Complex network measures of brain connectivity: uses and interpretations. *NeuroImage*, 52(3):1059–69, September 2010. ISSN 1095-9572. doi: 10.1016/j.neuroimage.2009.10.003. URL `http://www.ncbi.nlm.nih.gov/pubmed/19819337http://www.sciencedirect.com/science/article/pii/S105381190901074X`.

[60] F Ségonne, a M Dale, E Busa, M Glessner, D Salat, H K Hahn, and B Fischl. A hybrid approach to the skull stripping problem in MRI. *NeuroImage*, 22(3):1060–75, July 2004. ISSN 1053-8119. doi: 10.1016/j.neuroimage.2004.03.032. URL `http:`

//www.ncbi.nlm.nih.gov/pubmed/15219578.

[61] Sebastian Seung. *Connectome: How the Brain's Wiring Makes Us Who We Are*. 2013.

[62] J G Sled, a P Zijdenbos, and a C Evans. A nonparametric method for automatic correction of intensity nonuniformity in MRI data. *IEEE transactions on medical imaging*, 17(1):87–97, 1998. ISSN 0278-0062. doi: 10.1109/42.668698.

[63] Stephen M. Smith, Mark Jenkinson, Heidi Johansen-Berg, Daniel Rueckert, Thomas E. Nichols, Clare E. Mackay, Kate E. Watkins, Olga Ciccarelli, M. Zaheer Cader, Paul M. Matthews, and Timothy E J Behrens. Tract-based spatial statistics: Voxelwise analysis of multi-subject diffusion data. *NeuroImage*, 31:1487–1505, 2006. ISSN 10538119. doi: 10.1016/j.neuroimage.2006.02.024.

[64] Stamatios N. Sotiropoulos and Saad Jbabdi. Diffusion MR Tractography, 2014.

[65] Olaf Sporns. The human connectome: a complex network. *Annals of the New York Academy of Sciences*, 1224:109–25, April 2011. ISSN 1749-6632. doi: 10.1111/j.1749-6632.2010.05888.x. URL http://www.ncbi.nlm.nih.gov/pubmed/21251014.

[66] Olaf Sporns. Structure and function of complex brain networks. pages 247–262, 2013.

[67] Olaf Sporns, Giulio Tononi, and Rolf Kötter. The human connectome: A structural description of the human brain. *PLoS computational biology*, 1(4):e42, September 2005. ISSN 1553-7358. doi: 10.1371/journal.pcbi.0010042. URL http://dx.plos.org/10.1371/journal.pcbi.0010042http://www.pubmedcentral.nih.gov/articlerender.fcgi?artid=1239902&tool=pmcentrez&rendertype=abstract.

[68] M. R. Turner, V. Williams, Derek K. Jones, and P. N. Leigh. Neuroimaging in Amyotrophic Lateral Sclerosis. 1:319–337, 2006. doi: 10.1007/s13311-010-0011-3. URL http://orca.cf.ac.uk/35395/.

[69] University of Bristol MB ChB Year 3 Medicine and Surgery. Upper versus lower motor neurone signs, 2015. URL https://www.ole.bris.ac.uk/bbcswebdav/institution/FacultyofMedicineandDentistry/MBChB/HippocratesYear3MedicineandSurgery/Neurology-Presentingcomplaints/page_29.htm.

[70] David C Van Essen, Stephen M Smith, Deanna M Barch, Timothy E J Behrens, Essa Yacoub, and Kamil Ugurbil. The WU-Minn Human Connectome Project: an overview. *NeuroImage*, 80:62–79, October 2013. ISSN 1095-9572. doi: 10.1016/j.neuroimage.2013.05.041. URL http://www.sciencedirect.com/science/article/pii/S1053811913005351http://www.ncbi.nlm.nih.gov/pubmed/23684880.

[71] Esther Verstraete, Jan H Veldink, Rene C W Mandl, Leonard H van den Berg, and Martijn P van den Heuvel. Impaired structural motor connectome in amyotrophic lateral sclerosis. *PloS one*, 6(9):e24239, January 2011. ISSN 1932-6203. doi: 10.1371/journal.pone.0024239. URL http://www.pubmedcentral.nih.gov/articlerender.fcgi?artid=3166305&tool=pmcentrez&rendertype=abstract.

[72] Esther Verstraete, Daniel L Polders, René C W Mandl, Martijn P Van Den Heuvel, Jan H Veldink, Peter Luijten, Leonard H Van Den Berg, and Johannes Hoogduin. Multimodal tract-based analysis in ALS patients at 7T: a specific white matter profile? *Amyotrophic lateral sclerosis & frontotemporal degeneration*, 15(September 2013):84–92, 2014. ISSN 2167-9223. doi: 10.3109/21678421.2013.844168. URL http://www.ncbi.nlm.nih.gov/pubmed/24325276.

[73] D J Watts, D J Watts, S H Strogatz, and S H Strogatz. Collective dynamics of 'small-world' networks. *Nature*, 393(6684):440–2, 1998. ISSN 0028-0836. doi: 10.1038/30918. URL http://www.ncbi.nlm.nih.gov/pubmed/9623998.

[74] V J Wedeen, R P Wang, J D Schmahmann, T Benner, W Y I Tseng, G Dai, D N

Pandya, P Hagmann, H D'Arceuil, and a J de Crespigny. Diffusion spectrum magnetic resonance imaging (DSI) tractography of crossing fibers. *NeuroImage*, 41(4):1267–77, July 2008. ISSN 1053-8119. doi: 10.1016/j.neuroimage.2008.03.036. URL `http://www.ncbi.nlm.nih.gov/pubmed/18495497`.

[75] Lokesh C Wijesekera and P Nigel Leigh. Amyotrophic lateral sclerosis. *Orphanet journal of rare diseases*, 4:3, 2009. ISSN 1750-1172. doi: 10.1186/1750-1172-4-3.

[76] Wikipedia. Spinal muscular atrophies, 2015. URL `http://en.wikipedia.org/wiki/Spinal_muscular_atrophies`.

[77] Mingrui Xia, Jinhui Wang, and Yong He. BrainNet Viewer: a network visualization tool for human brain connectomics. *PloS one*, 8(7):e68910, January 2013. ISSN 1932-6203. URL `http://www.plosone.org/article/info:doi/10.1371/journal.pone.0068910#pone-0068910-g009`.

[78] Andrew Zalesky, Alex Fornito, and Edward T Bullmore. Network-based statistic: identifying differences in brain networks. *NeuroImage*, 53(4):1197–207, December 2010. ISSN 1095-9572. doi: 10.1016/j.neuroimage.2010.06.041. URL `http://www.sciencedirect.com/science/article/pii/S1053811910008852http://www.ncbi.nlm.nih.gov/pubmed/20600983`.

[79] Andrew Zalesky, Luca Cocchi, Alex Fornito, Micah M Murray, and Ed Bullmore. Connectivity differences in brain networks. *NeuroImage*, 60(2):1055–62, April 2012. ISSN 1095-9572. doi: 10.1016/j.neuroimage.2012.01.068. URL `http://www.ncbi.nlm.nih.gov/pubmed/22273567`.